Viral modulation of type II interferon increases T cell adhesion and virus spread

Carina Jürgens[1,¶], George Ssebyatika[1,2], Sarah Beyer[1,¶], Nina Plückebaum[1], Kai A. Kropp[1], Víctor González-Motos[1,3,¶], Birgit Ritter[1], Heike Böning[1], Eirini Nikolouli[4,5,6,7], Paul R. Kinchington[8], Nico Lachmann[4,5,6,7], Daniel Pearce Depledge[1,7,9], Thomas Krey[1,2,7,10,11] and Abel Viejo-Borbolla[1,7*].

[1] Institute of Virology, Hannover Medical School, Hannover 30625, Germany
[2] Institute of Biochemistry, University of Lübeck, Lübeck 23562, Germany
[3] University of Veterinary Medicine Hannover, Foundation, Hannover 30559, Germany
[4] Department for Pediatric Pneumology, Allergology and Neonatology, Hannover Medical School, Hannover 30625, Germany
[5] Fraunhofer Institute for Toxicology and Experimental Medicine (ITEM), Nikolai-Fuchs-Str. 1, 30625 Hannover, Germany
[6] Biomedical Research in Endstage and Obstructive Lung Disease Hannover (BREATH), German Center for Lung Research (DZL), Hannover, Germany.
[7] Excellence Cluster 2155 RESIST, Hannover Medical School, Hannover 30625, Germany
[8] Department of Ophthalmology and of Molecular Microbiology and Genetics, University of Pittsburgh, Pittsburgh, PA, United States
[9] German Center for Infection Research (DZIF), partner site Hannover-Braunschweig, Hannover, Germany
[10] Centre for Structural Systems Biology (CSSB), 22607 Hamburg, Germany
[11] German Center for Infection Research (DZIF), Partner Site Hamburg-Lübeck-Borstel-Riems, 22607 Hamburg, Germany

[¶] Current addresses:
CJ, Department of Gastroenterology, Hepatology, Infectious Diseases and Endocrinology, Hannover Medical School, Hannover 30625, Germany
SB, Institute for Medical Microbiology and Hospital Epidemiology, Hannover Medical School, Hannover 30625, Germany
VGM, Firalis SA, 68330 Huningue, France

* correspondence: viejo-borbolla.abel@mh-hannover.de (A.V.-B.)

Abstract

During primary infection, varicella zoster virus (VZV) infects epithelial cells in the respiratory lymphoid organs and mucosa. Subsequent infection of lymphocytes, T cells in particular, causes primary viremia allowing systemic spread throughout the host, including the skin. This results in the expression of cytokines, including interferons (IFNs) which partly limit primary infection. VZV also spreads from skin keratinocytes to lymphocytes prior to secondary viremia. How VZV infects lymphocytes from epithelial cells while evading the cytokine response has not been fully established. Here, we show that VZV glycoprotein C (gC) binds IFN-γ and modifies its activity. Transcriptomic analysis revealed that gC in combination with IFN-γ increased the expression of a small subset of IFN-stimulated genes (ISGs), including intercellular adhesion molecule 1 (*ICAM1*), as well as several chemokines and immunomodulatory genes. The higher ICAM1 protein level at the plasma membrane of epithelial cells resulted in lymphocyte function-associated antigen 1 (LFA-1)-dependent T cell adhesion. This gC activity required a stable interaction with IFN-γ and signalling through the IFN-γ receptor. Finally, the presence of gC during infection increased VZV spread from epithelial cells to peripheral blood mononuclear cells. This constitutes the discovery of a novel strategy to modulate the activity of IFN-γ, inducing the expression of a subset of ISGs, leading to enhanced T cell adhesion and virus spread.

Keywords: Interferon gamma; varicella zoster virus; immunomodulation; biased signalling; ICAM1; LFA-1; T cell adhesion; virus spread

Introduction

Respiratory inhalation of varicella zoster virus (VZV) in naïve persons results in infection of epithelial cells of the respiratory mucosa and lymphoid organs of the Waldeyer's tonsillar ring. The close interaction with immune cells, including T cells, results in their infection, which then disseminates VZV systemically in the body[1, 2, 3]. VZV modifies the receptor expression profile of infected T cells, increasing the level of proteins that facilitate T cell homing to the skin and basal stem niches of hair follicles[4], where infectious virus is transferred to keratinocytes[5]. A slow infection partly controlled by innate responses ultimately leads to the eruption of virus at the differentiating surface epithelia, resulting in the typical chickenpox rash. At later stages of infection, another wave of migrating mononuclear cells reaches the skin and VZV spreads from keratinocytes to lymphocytes, causing secondary viremia[5, 6]. The processes and mechanisms that lead to VZV spread from epithelial cells to lymphocytes are not well understood.

VZV is human specific and animal models do not fully reflect VZV pathogenesis. However, the use of severe combined immunodeficiency (SCID) mice xenografted with human skin and dorsal root ganglia support the relevance of T cell migration for VZV spread and pathogenesis *in vivo* [2, 5, 7]. Lymphocyte migration is a complex process that requires the concerted action of different proteins including chemokines, adhesion molecules and integrins. Chemokine interaction with their receptors on the T cell leads to activation of integrins, such as lymphocyte function-associated antigen 1 (LFA-1)[8]. Similarly, chemokines and interferon-gamma (IFN-γ) increase the expression of intercellular adhesion molecule 1 (ICAM1) on the endothelium and epithelium[9]. The interaction between LFA-1 and ICAM1 facilitates firm T cell adhesion and transmigration[9, 10]. The ICAM1 – LFA-1 interaction plays a key role in the formation of

the immunological synapse[11], and in the cytotoxic T cell response that kills infected cells[12, 13].

The innate response to viral infections includes the expression of type I, II and III IFNs, key antiviral cytokines that bind specific receptors to induce the expression of hundreds of IFN stimulated genes (ISGs). The expressed ISGs and their level of expression are characteristic for each IFN, and even vary for the same IFN, depending on the cell type[14]. Interestingly, the mode of binding of IFN-γ to the IFN-γ receptor (IFNGR) also influences the induction of ISGs, as seen with recombinant IFNGR agonists that induce biased signalling and differential expression of ISG subsets[15]. One of the differentially expressed ISGs upon binding of a biased agonist is *ICAM1*[15].

Due to the role of chemokines and IFNs in the antiviral response, viruses have devised many strategies to modulate their activities. Herpesviruses and poxviruses express viral chemokine binding proteins (vCKBP) that bind and modulate chemokine function[16, 17]. Most vCKBP discovered to date inhibit chemokine function with the exception of HSV glycoprotein G and VZV glycoprotein C (gC), which both enhance chemokine-mediated migration of leukocytes[16, 17, 18, 19, 20]. VZV gC is not required for growth in cell culture but is important in skin infection[21]. Until now, viral proteins that bind soluble IFN have only been discovered in poxviruses[22, 23]. These IFN-binding proteins bind IFN with high affinity and thereby compete with the interaction with their receptor, inhibiting IFN activity, and their deletion or mutation severely attenuates the virus *in vivo*[24, 25, 26].

Since gC increases T cell chemotaxis[18], a process influenced by chemokines and IFNs, and is relevant for efficient spread in human skin[5, 21], we sought to investigate whether gC could modulate cytokine activity and spread from epithelial to T cells. We show here that VZV gC binds type II IFN with high affinity. Contrary to what has been observed for poxviruses, VZV gC did not inhibit IFNGR signalling and induction of

ISGs. Interestingly, VZV gC binding resulted in a biased activation of IFN-γ ISG stimulation that resulted in increased expression of a subset of ISGs, including *ICAM1*. Increased levels of ICAM1 at the plasma membrane facilitated adhesion of T cells expressing LFA-1. We also observed more efficient VZV spread from HaCaT to Jurkat cells and to peripheral blood mononuclear cells (PBMCs) when gC was expressed during infection. Collectively, we report a previously undescribed activity of viral modulation of IFN-γ that results in the induction of biased ISG expression, increasing ICAM1 levels, T cell adhesion and virus spread.

Results

VZV gC binds type II IFN.

VZV gC is a known important virulence factor in *in vivo* infections of human tissues in SCID mice[21] that enhances chemokine-dependent migration[18]. Due to the relevance of IFNs in antiviral responses and lymphocyte adhesion, we performed a surface plasmon resonance (SPR) binding screening with human IFNs. VZV gC is a type I transmembrane protein with an ectodomain (ECD) containing an N-terminal repeated domain (termed R2D) and a larger C-terminal region (formerly termed immunoglobulin-like domain (IgD))[18], a transmembrane region, and a very short cytoplasmic tail (Fig. 1A). We used Phyre2 (http://www.sbg.bio.ic.ac.uk/~phyre2/html/page.cgi?id=index) server predictions of the secondary structure of the gC ECD to design truncated gC expression constructs. We expressed, purified (Suppl. Fig. 1), and immobilised gC constructs onto CM5 Biacore chips. $gC_{P23\text{-}V531}$, corresponding to the full-length ECD, bound IFN-β, IFN-ω, IFN-γ, IFN-λ1 and IFN-λ2 but did not bind IFN-α and tumor necrosis factor alpha (TNF-α) (Fig. 1B). To identify the region required for interaction with IFN, and to confirm the lack of interaction with different IFN-α subtypes, we immobilised $gC_{S147\text{-}V531}$, $gC_{Y322\text{-}S523}$ and $gC_{V419\text{-}S523}$ on a CM5 chip. All three truncations of the gC ECD bound to the different IFNs, except the IFN-α subtypes (Suppl. Fig. 2A). To confirm the gC – IFN interactions, we used grating-coupled interferometry (GCI) to perform repeated analyte pulses of increasing duration (RAPID) experiments. We immobilised $gC_{S147\text{-}V531}$, $gC_{Y322\text{-}S523}$ and $gC_{V419\text{-}S523}$ on a DXH chip and injected IFN-β, IFN-γ, IFN-λ1, IFN-λ2, IFN-ω and TNF-α as negative control. Injection of IFN-γ on chips immobilised with $gC_{S147\text{-}V531}$ and $gC_{Y322\text{-}S523}$ led to a high response, while the response for $gC_{V419\text{-}S523}$ was very low, suggesting a low affinity interaction or no binding (Suppl. Fig. 2B, top row). Very low or even no responses were observed for the other tested IFNs against the different gC constructs, suggesting that gC bound type I and

III IFNs weaker than type II IFN (Suppl. Fig. 2B, notice the different scales in the Y axis). Along this line, our efforts to investigate the effect of gC on type I and III IFN did not show any influence of gC on their activities (data not shown). Based on these results, we hypothesized that only the gC – IFN-γ interaction may be of functional relevance.

VZV gC induces biased expression of IFN-γ-induced ISGs.

We employed an unbiased approach to determine the functional impact of gC on IFN-γ by analysing the transcriptome of HaCaT, a keratinocyte cell line, upon incubation with $gC_{S147\text{-}V531}$ and IFN-γ, both alone and in combination. Total RNA was extracted at 4 hours post-treatment to reduce the potential impact of feedback loops in the results and subsequently enriched for polyadenylated RNA. Following sequencing, quality control, alignment of reads to the host genome, and the generation of gene abundance counts, we generated a principal component analysis (PCA) which showed that the different experimental groups separated based on IFN-γ treatment (Suppl. Fig. 3A). We determined RNA fold changes comparing the different groups and their significances using DESeq2. Genes were considered significantly differentially expressed between the experimental conditions if they had an adjusted *P* value lower than 0.05 and a log2-fold change greater than 0.58 (equivalent to a 1.5-fold change). The addition of IFN-γ significantly modulated the expression of 776 genes in HaCaT cells (Suppl. Fig. 3B). The combination of $gC_{S147\text{-}V531}$ and IFN-γ raised the number of significantly regulated genes to 831 (Suppl. Fig. 3C), while $gC_{S147\text{-}V531}$ alone induced significant expression of just 16 genes (Suppl. Fig. 3D), among them chemokines, signalling molecules and the adhesion molecule *ICAM1.* When comparing the impact of adding $gC_{S147\text{-}V531}$ and IFN-γ together versus IFN-γ alone, we observed a significant increase in the expression of 28 genes and 1 pseudogene (Suppl. Fig. 3E).

We generated a heatmap showing the 42 genes with a significant expression change after addition of gC (Fig. 2A,B). Dendrograms showed the same treatment conditions clustered together, indicating the reproducibility of the results (Fig. 2B). The majority of changes induced by IFN-γ, gC or both resulted in higher gene expression compared to the mock control (Suppl. Fig. 4A). When comparing the effect of 'both vs. IFN-γ', we did not observe significantly downregulated genes. Next, we plotted the log2-fold changes of the significantly regulated genes against each other (Suppl. Fig. 4B). We defined a corridor (grey lines) in which the fold change was less than 1.5-fold. Genes outside this corridor were significantly differentially regulated by gC. A distinct set of genes, including chemokines (*CXCL10* and *CXCL11*), pro-inflammatory cytokines (*IL6* and *IL32*), the E3 ubiquitin ligase *NEURL3*[27] but also *IL4I1*, an enzyme involved in immunosuppression[28], and a pseudogene (*OR2I1P*), were strongly regulated upon the combined treatment, but not when gC was added alone.

The log2-fold change is only a relative value and does not depict absolute changes that could largely differ depending on the baseline gene expression in the presence or absence of IFN-γ. Therefore, we calculated and plotted the effect size for the 42 significantly regulated genes by gC (Fig. 2C-F). In addition to the four major groups observed in the heatmap (Fig. 2B), we divided the genes into two categories, those that were regulated by IFN-γ in our datasets and those that were not. Among the genes that were not regulated by IFN-γ, the effect size of *IL4I1* was 7.4-fold higher in the gC plus IFN-γ condition than with gC alone (Fig. 2D). The effect on *IL4I1* expression seen in the 'gC vs. mock' comparison was not statistically significant, while it was when comparing 'both vs. IFN-γ'. This result, together with the fact that IFN-γ did not upregulate *IL4I1* and due to its role in immune modulation[28], highlights *IL4I1* as an interesting target for further studies. Additionally, among the genes not regulated by IFN-γ, we observed seven genes with more than a 1.5-fold difference in their effect

sizes, when comparing the effect size of gC in the presence or absence of IFN-γ. These include chemokines and transcriptional regulators: *CCL20*, *CITED4*, *CXCL2*, *CXCL3*, *CXCL8*, *DUSP5*, and *HIVEP2* (Fig. 2D-F).

Interestingly, the picture was different when looking at the genes regulated by IFN-γ: 82% of the genes showed differences for the two comparisons ("gC vs. mock" and "both vs. IFN-γ", Fig. 2C, D, F). The co-stimulation with gC and IFN-γ upregulated the expression of eleven genes and one pseudogene. Intriguingly, five of these gene products are involved in T cell migration: ICAM1 and the chemokines CCL2, CXCL9, CXCL10 and CXCL11. For *ICAM1*, gC led to about 26-fold higher effect size in the presence of IFN-γ compared to the condition without IFN-γ.

Overall, the transcriptomic analysis shows that $gC_{S147\text{-}V531}$ alone induced the expression of few genes, some of them also regulated by IFN-γ while others were not. $gC_{S147\text{-}V531}$ did not induce a general enhancement of IFN-γ-stimulated genes but increased expression of a subset of specific genes, especially those involved in chemokine-mediated migration and adhesion. This suggests that gC induces a biased expression of ISGs.

VZV gC modifies the activity of IFN-γ, leading to higher expression of ICAM1.

Since gC is a known vCKBP that modulates chemotaxis, we focused mainly on the genes involved in migration and cell adhesion. We confirmed by RT-qPCR the increased expression of *CXCL8*, *CXCL9*, *CXCL10*, *CXCL11*, *IL4I1,* and *ICAM1* in the presence of gC and IFN-γ (Suppl. Fig 5 and 6A). ICAM1 is an important adhesion molecule for cell migration. Therefore, we quantified ICAM1 mRNA and protein at different time points post-incubation of HaCaT cells with IFN-γ or $gC_{S147\text{-}V531}$ alone or the combination of both. *ICAM1* mRNA expression level peaked at 4 h post-stimulation (Suppl. Fig. 6A). There was no detectable ICAM1 protein in the absence of IFN-γ

treatment or in the presence of $gC_{S147-V531}$ alone at any time post-stimulation (Suppl. Fig. 6B). However, addition of IFN-γ increased ICAM1 protein levels from 4 hours post-stimulation and the combination of IFN-γ and $gC_{S147-V531}$ enhanced IFN-γ-induced ICAM1 transcripts significantly from 6 hours and total protein from 10 hours post-incubation, respectively, reaching about 3-fold more ICAM1 protein at 10 hours post-stimulation (Suppl. Fig. 6). The increase in *ICAM1* expression obtained in the RNA-seq was 1.44-fold higher when comparing co-stimulated cells versus IFN-γ-stimulated cells at 4 hours post-stimulation. This fold-change is similar to the 1.37-fold change observed in the RT-qPCR assay (Suppl. Fig. 6A), and confirmed our previous observations of gC enhancing the IFN-γ-induced *ICAM1* mRNA levels.

We hypothesised that gC – IFN-γ interaction would also increase ICAM1 at the plasma membrane. To address this hypothesis, we incubated HaCaT cells with IFN-γ alone or together with $gC_{S147-V531}$ and determined the level of ICAM1 at the plasma membrane 24 hours later by flow cytometry (Suppl. Fig. 7A). We also investigated the effect of gC on another ISG, major histocompatibility complex II (MHCII), and determined which gC region was required to modulate IFN-γ-mediated ICAM1 and MHCII levels (Fig. 3). MHCII is a known component of the immunological synapse. $gC_{S147-V531}$ and $gC_{Y322-S523}$, enhanced IFN-γ-induced levels of ICAM1, while only $gC_{S147-V531}$ had a similar impact on MHCII (Fig. 3A,B). Interestingly, $gC_{Y419-S523}$ did not enhance IFN-γ-mediated induction of ICAM1 and MHCII (Fig. 3A,B). We then determined whether the observed effect was cell-type specific. Addition of IFN-γ and $gC_{S147-V531}$ increased the level of ICAM1 compared to the IFN-γ only treatment in HaCaT, MeWo, A549 and Jurkat cells, suggesting that the effect was not cell-type dependent (Suppl. Fig. 7B). IFN-γ also increased MHCII levels in HaCaT and MeWo cells, although to a lower extent than ICAM1 (Fig. 3B and Suppl. Fig. 7C). There was no increase in the level of MHCII in

A549 and Jurkat cells, in any tested conditions, in line with reports from the literature[29, 30].

These results showed that VZV gC enhanced IFN-γ-mediated ICAM1 and MHCII protein level at the plasma membrane in different cell types. The effect on MHCII was considerably lower than that observed for ICAM1. In all the tested conditions, addition of $gC_{S147\text{-}V531}$ or $gC_{Y322\text{-}S523}$ alone did not significantly enhance the protein levels of ICAM1 or MHCII, suggesting that the effect was not due to the presence of a contaminant that led to expression of these two proteins. Moreover, different cells responded to a different extend to IFN-γ and $gC_{S147\text{-}V531}$, probably reflecting differences in expression levels of IFNGR or downstream proteins.

Taken together with results presented so far, these results show that VZV gC increases both mRNA and protein levels of ICAM1 in the presence of IFN-γ and confirm an enhancing effect of gC on IFN-γ-induced ICAM1 expression. In addition, residues Y322-S523 are required for this function.

gC activity requires signalling through the IFNGR.

The previous results suggested that the mechanism of gC activity involves binding to IFN-γ and signalling through the IFNGR. To confirm this, we employed an antibody that neutralises IFNGR1[31]. Addition of IFN-γ increased ICAM1 and MHCII levels on the plasma membrane of HaCaT cells and the combination of IFN-γ plus $gC_{S147\text{-}V531}$ or $gC_{Y322\text{-}S523}$ further increased these levels (Fig. 3C, D). The neutralising antibody inhibited IFN-γ activity, and the increase mediated by $gC_{S147\text{-}V531}$ or $gC_{Y322\text{-}S523}$, while the isotype control did not (Fig. 3C, D).

To complement these results, we also employed iPSC-derived macrophages from a healthy donor and a patient suffering Mendelian susceptibility to mycobacterial disease (MSMD) due to a deficiency of IFNGR2[32]. In the iPSC-derived macrophages obtained

from a healthy individual, the enhancement of ICAM1 by co-stimulation with gC and IFN-γ occurred with faster kinetics than in the tested cell lines, peaking at 8 h post stimulation, whereas MHCII induction by IFN-γ was completely abolished by addition of gC (Suppl. Fig. 8A). Nevertheless, lack of IFNGR2 chain also abolished the enhancement of ICAM1 surface levels by IFN-γ alone and together with gC (Suppl. Fig. 8B). Interestingly, in this cell type, gC alone induced a significant upregulation of ICAM1 at 8 hours post-stimulation, independent of signalling via the IFNGR2, by an unknown mechanism.

Overall, these results showed that the synergism of VZV gC and IFN-γ on ICAM1 and MHCII expression required signalling through the IFNGR complex. They also suggest that gC could bind and signal through another receptor to induce ICAM1 protein expression in macrophages, independently of IFNGR signalling.

VZV gC binds IFN-γ through its glycosaminoglycan-binding site

The observation that gC did not inhibit IFN-γ and that it required signalling through the IFNGR to increase ICAM1 and MHCII protein levels suggest that gC did not interact with the IFNGR-binding site of IFN-γ. Since IFN-γ also binds to glycosaminoglycans (GAGs), we addressed whether gC interacted with IFN-γ through its GAG-binding regions by competing the interaction with increasing concentrations of heparin, heparan sulfate and chondroitin sulfate A and B (Suppl. Fig. 9). The presence of GAGs interfered with the ability of gC to bind IFN-γ. The most effective competitor was heparin (Suppl. Fig. 9A), inhibiting 50% of binding with a ratio of 1:0.1 (IFN-γ:GAG; weight:weight ratio), while the other three GAGs required a ratio of about 1:10 (Suppl. Fig. 9B,C,D). These results suggested that gC bound IFN-γ through its GAG-binding regions.

VZV gC increases IFN-γ-mediated T cell adhesion

ICAM1 binding to LFA-1 on T cells facilitates their adhesion on endothelial and epithelial cells. We hypothesised that the increased plasma membrane level of ICAM1 on HaCaT cells upon incubation with IFN-γ and gC could increase T cell adhesion. Therefore, we performed adhesion assays with HaCaT and Jurkat cells (Fig. 4A). Addition of IFN-γ to HaCaT cells increased the number of adhered Jurkat cells by 2.3-fold compared to the unstimulated control (Fig. 4B). Addition of IFN-γ plus $gC_{S147\text{-}V531}$ increased Jurkat cell adhesion by 2.7-fold compared to IFN-γ and 6.1-fold compared to the unstimulated control, while $gC_{S147\text{-}V531}$ alone did not. $gC_{S147\text{-}V531}$ increased IFN-γ-dependent cell adhesion in a dose dependent manner when a constant concentration of IFN-γ (5 ng/mL) was employed (Fig. 4C). We then determined which gC region was responsible for this effect. Both $gC_{S147\text{-}V531}$ and $gC_{Y322\text{-}S523}$ increased the adhesion of Jurkat to HaCaT cells upon incubation with IFN-γ, while $gC_{Y419\text{-}S523}$ did not (Fig. 4D), correlating with their binding properties and impact on IFN-γ-mediated ICAM1 expression (Suppl. Fig. 2 and Fig. 3A). To determine the role of the ICAM1 – LFA-1 interaction in this process, we employed Jurkat cells lacking LFA-1 expression (LFA-1 KO). The absence of LFA-1 resulted in very low adhesion to HaCaT cells in all conditions, irrespective of the presence of IFN-γ and $gC_{S147\text{-}V531}$ (Fig. 4E).

Overall, these results indicated that the enhanced IFN-γ-dependent ICAM1 expression induced by gC resulted in higher adhesion of T cells through LFA-1. In line with the ICAM1 upregulation data, these experiments also showed that amino acids Y322-S523 of gC are required for this activity. Importantly, gC did not increase T cell adhesion in the absence of IFN-γ.

The increase in ICAM1 expression and T cell adhesion requires a stable gC - IFN-γ interaction

The $gC_{S147\text{-}V531}$ and $gC_{Y322\text{-}S523}$ constructs enhanced ICAM1 expression and T cell adhesion, while $gC_{Y419\text{-}S523}$ did not. Moreover, the binding analyses suggest that $gC_{Y419\text{-}S523}$ bound IFN-γ worse than $gC_{S147\text{-}V531}$ and $gC_{Y322\text{-}S523}$ (Suppl. Fig. 2). To better characterize the interaction between the three gC constructs and IFN-γ, we performed multicycle kinetic experiments by SPR (Suppl. Fig. 10A and Suppl. Table 1). The curvature of the sensorgrams from kinetic experiments suggested that the interaction between gC and IFN-γ deviates from a simple 1:1 binding, especially for $gC_{S147\text{-}V531}$ and $gC_{Y322\text{-}S523}$ (Suppl. Fig. 10A). The heterogenous interaction can be described by at least two components (Suppl. Fig. 10B), one transient and another more stable. The transient component contributes more to the interaction at higher than at lower IFN-γ concentrations (Suppl. Fig. 10B) and seems sensitive to increasing salt concentrations (Suppl. Fig. 10C), indicating the relevance of electrostatic interactions. $gC_{Y419\text{-}S523}$ interacts with IFN-γ transiently, since the more stable interaction is not observed (Suppl. Fig. 10A, right panel and B). The RAPID experiments (Suppl. Fig. 2B) also suggested a weaker binding of $gC_{Y419\text{-}S523}$ to IFN-γ, as observed by the very low responses.

Since we observed two modes of interaction with $gC_{S147\text{-}V531}$ and $gC_{Y322\text{-}S523}$, we employed a heterogenous ligand fit model, while we applied a 1:1 fitting for $gC_{Y419\text{-}S523}$ - IFN-γ, since only the transient interaction was detected (Suppl. Fig. 10D and Suppl. Table 1, 2). The results indicated that both $gC_{S147\text{-}V531}$ and $gC_{Y322\text{-}S523}$ bound IFN-γ in a similar manner. We observed a transient interaction with an off-rate (Kd1) in the range of 4×10^{-2}/s and a more stable interaction with a slower off-rate (Kd2). (Suppl. Table 1, 2). The transient interaction of $gC_{Y419\text{-}S523}$ and IFN-γ had a fast off-rate of about 2×10^{-2}/s (Suppl. Table 1), resembling the off-rate of the transient interaction of the longer gC constructs. Together with our functional observations, these data indicate

that the stable, higher affinity interaction with IFN-γ, that occurs only with the $gC_{S147-V531}$ and $gC_{Y322-S523}$, is important for gC function.

IFN-γ-mediated ICAM1 expression increases in epithelial cells infected with VZV

We obtained all the previous data with recombinant, purified gC constructs. In a next step, we addressed whether gC expressed during VZV infection played a similar role as the purified protein. We initially determined the level of ICAM1 during infection of HaCaT cells using a recombinant bacterial artificial chromosome (BAC)-derived VZV pOka strain expressing monomeric enhanced green fluorescent protein (GFP) under the control of the ORF57 promoter (pOka-Δ57-GFP). After two days of infection with pOka-Δ57-GFP, we stimulated the cells with IFN-γ for another day and then quantified ICAM1 protein levels by flow cytometry (Suppl. Fig. 11A). Initially, we gated on live cells for each well, without considering the GFP expression and hence the infection status (Suppl. Fig. 11B). Cells without IFN-γ had low level of ICAM1 expression, irrespective of the presence or absence of VZV in the culture. Upon stimulation with IFN-γ, there was more ICAM1 in all samples, and a tendency toward higher ICAM1 levels in the VZV- than in mock-infected cultures (Suppl. Fig. 11B). In the VZV-inoculated cultures, we discriminated between uninfected bystander cells and productively VZV-infected GFP positive (GFP^+) cells. We separated the infected cells into GFP^{high} and GFP^{low} populations, resembling cells with high and low viral replication and viral gene expression, respectively. IFN-γ treatment reduced slightly the number of infected cells, reducing the percentage of GFP^{high} cells and slightly increasing that of GFP^{low} cells compared to the mock-treated control, due to the inhibitory effect of IFN-γ on VZV replication, as previously shown[33, 34] (Suppl. Fig. 11C). Comparing the fold-change by IFN-γ, we observed a significant higher fold-change of ICAM1 in the VZV-inoculated culture, independent of the cells being uninfected bystanders or

productively infected cells (Suppl. Fig. 11D). The productively infected cells showed higher fold-change in ICAM1 upon addition of IFN-γ than the uninfected bystander cells, and this was more pronounced in the GFP^{low} cells (Suppl. Fig. 11E). Interestingly, ICAM1 induction was lower in GFP^{high} cells, indicating high virus production, in line with previous results showing that VZV infection inhibits ICAM1 expression[35, 36]. Taken together, these results indicate that VZV-infected HaCaT cells express more ICAM1 than mock-infected cells upon IFN-γ stimulation.

VZV gC increases T cell adhesion during infection

To investigate the relevance of the IFN-γ-mediated ICAM1 upregulation in the context of infection and to address the role of gC, we employed two recombinant, BAC-derived VZV pOka viruses: pOka-gC-GFP and pOka-ΔgC-GFP. In both viruses, the monomeric enhanced GFP signal is expressed from the promoter of *ORF14* (encoding gC) (Suppl. Fig. 12). Since *ORF14* is a late gene, only expressed after VZV DNA replication, the presence of GFP indicates productive infection. VZV pOka-ΔgC-GFP was previously generated and characterized[18]. To generate pOka-gC-GFP, we fused GFP to *ORF14* using *en passant* mutagenesis[37], similar to the generation of the pOka-ΔgC-GFP (Suppl. Fig. 12A). Both viruses replicated with similar kinetics in HaCaT cells (Suppl. Fig. 12B), indicating that lack of gC did not affect VZV replication *in vitro*, as previously shown[18, 38]. Moreover, the level of GFP detected was similar for both viruses. Therefore, we used GFP detection as a surrogate of productive VZV infection. We then performed cell adhesion assays on HaCaT cells infected with the same plaque forming units (PFU) of pOka-gC-GFP or pOka-ΔgC-GFP. At two days post-infection (dpi), we stimulated the cells with IFN-γ for another day and added Hoechst-labelled Jurkat cells. We imaged the cells and measured the mean GFP and Hoechst intensities (Fig. 5A). Analysis of the GFP levels at 3 dpi showed that both viruses

replicated similarly in HaCaT cells (Fig. 5B), also after addition of IFN-γ. This indicated once again that gC did not reduce the antiviral effect of IFN-γ. Since the number of counted nuclei correlated with the mean Hoechst signal, we used the mean fluorescence intensities as a surrogate for adhered cells. The number of infected cells may vary between region of interests (ROI). Therefore, we normalised the Hoechst signal to the respective GFP signal for each ROI. With increasing IFN-γ concentrations, we observed a slight increase in cell adhesion upon infection with both viruses with a tendency of higher Jurkat adhesion in the cells infected with pOka-gC-GFP compared to those infected with pOka-ΔgC-GFP (Fig. 5C). We then calculated the ratio of the Hoechst/GFP value from pOka-gC-GFP to the pOka-ΔgC-GFP and normalised it to mock-treated cells (Fig. 5D). This analysis showed that there was an IFN-γ dose-dependent increase in Jurkat cell adhesion when HaCaT cells were infected with VZV pOka-gC-GFP compared to pOka-ΔgC-GFP. Notably, the adhered cells clustered around the productively infected cells (GFP^+ cells; Fig. 5E), but also adhered to the bystander cells. This observation is in line with the ICAM1 upregulation assay, where the GFP^{low} and the bystander cells expressed higher ICAM1 levels than the GFP^{high} cells (Suppl. Fig. 11). Overall, these results suggest that the expression of gC during VZV infection of HaCaT cells facilitates the adhesion of Jurkat cells.

VZV gC facilitates spread from epithelial cells to T cells

We hypothesised that the higher ICAM1 expression and T cell adhesion mediated by the combination of IFN-γ and gC may result in more efficient VZV spread to T cells. To this end, we performed an adhesion experiment in which the co-culture of HaCaT and Jurkat cells were maintained for one to two days after cell adhesion. Then, the GFP levels in both populations were analysed by flow cytometry. The amount of GFP^+ HaCaT cells was similar between both gC-expressing and ΔgC viruses, with

approximately 21 – 23% of infected cells in IFN-γ untreated cultures (Fig. 6A). The amount of GFP$^+$ HaCaT cells for both viruses declined to about 17% and 12%, upon incubation with 0.5 and 5 ng/mL of IFN-γ, respectively. In the untreated co-culture, the amount of GFP$^+$ Jurkat cells, indicative of VZV infection, was about 2.5% for the pOka-gC-GFP virus and about 2.0% for the pOka-ΔgC-GFP virus (Fig. 6B). We observed an IFN-γ-dependent decrease of GFP$^+$ Jurkat cells for both viruses, but a tendency indicating less infected Jurkat cells for the pOka-ΔgC-GFP compared to the pOka-gC-GFP. Since only infected HaCaT cells can transmit the virus and the amount of infected HaCaT cells decreased with IFN-γ treatment, we calculated the ratio of GFP$^+$ Jurkat cells to GFP$^+$ HaCaT cells (Fig. 6C). Again, we observed a tendency of better transmission for the pOka-gC-GFP virus compared to the pOka-ΔgC-GFP virus. To better judge the effect of IFN-γ treatment, the ratio between pOka-gC-GFP to pOka-ΔgC-GFP was calculated from the Jurkat/HaCaT ratio to obtain the fold change by gC (Fig. 6D). These data indicated that the pOka-gC-GFP virus spreads better than the pOka-ΔgC-GFP from HaCaT to Jurkat cells in the presence of IFN-γ.

To increase the relevance of our results, we repeated these experiments with human peripheral blood mononuclear cells (PBMCs) obtained from healthy donors. As before, the percentage of GFP$^+$ HaCaT cells dropped for both viruses upon addition of IFN-γ in a dose dependent manner (Fig. 6E). However, while pOka-gC-GFP virus spread from HaCaT cells to PBMCs, the pOka-ΔgC-GFP virus barely spread at all to PBMC (Fig. 6F). This was even more obvious, when calculating the GFP$^+$ PBMC/HaCaT ratio and the fold change by gC, showing that the pOka-gC-GFP virus spread better to PBMCs than the pOka-ΔgC-GFP virus (Fig. 6G,H). Taken together, the results suggested that gC is critical to facilitate virus transmission from HaCaT cells to PBMCs, in both the absence and presence of IFN-γ.

Discussion:

Viruses have evolved a variety of mechanisms to inhibit or modulate the innate and adaptive immune responses to establish productive infection and spread in the host, particularly under low virus input. One such strategy, employed by herpes- and poxviruses, consists of the expression of type I transmembrane or secreted viral proteins that bind cytokines to modulate or alter their activities. On many occasions, such viral proteins act as decoy receptors, inhibiting the immune response[39, 40]. However, here we show that the vCKBP gC binds IFN-γ, without apparently inhibiting IFN activity and the stimulation of ISGs. On the contrary, gC binding to IFN-γ led to induction of an IFN-γ-mediated biased gene expression in which the expression of few ISGs was more upregulated. This set included *ICAM1*, which was increased at the mRNA and protein level in keratinocytes, facilitating Jurkat cell adhesion and resulting in better infection of both Jurkat cells and PBMCs. We hypothesise that the gC - IFN-γ interaction facilitates VZV spread from epithelial to T cells, both at the respiratory lymphoid epithelium and prior to secondary viremia, when mononuclear cells are recruited to the infected skin[5, 6, 7].

VZV gC combined with IFN-γ induced differential expression of a subset of several genes. Some of these genes (*CCL2*, *CCL20*, *CXCL2*, *CXCL3*, *CXCL9*, *CXCL10* and *CXCL11*) play key roles in chemotaxis, an activity that VZV gC also enhances through its interaction with chemokines[18], and cell adhesion (*ICAM1*). VZV gC also increased IFN-γ-mediated induction of other genes, like *IL4I1*, whose protein product downregulates the immune response[28]. Secretion of IL4I1 at the immunological synapse is known to decrease TCR activation and signalling, resulting in inhibition of T cell proliferation and facilitating the development of regulatory T cells[28]. The increased ICAM1 levels and its interaction with LFA-1 could also affect T cell differentiation. Signalling through ICAM1 tends to result in expression of pro-

478 inflammatory cytokines[41], and LFA-1 activation in the context of TCR signalling is
479 relevant for T cell differentiation into effector phenotypes[42]. We do not know yet
480 whether the differential gene expression due to gC-IFN-γ interaction modulates T cell
481 differentiation and/or activity. This could be relevant in the context of VZV infection of
482 T cells and the subsequent VZV directed modulation of their receptor expression profile
483 that results in T cells with a skin homing, effector memory phenotype[4]. Interestingly,
484 despite the infected T cells having an effector phenotype[4], they do not seem to
485 eliminate the virus, but rather mediate the transport of VZV to the skin and facilitate
486 efficient spread into keratinocytes[5]. We speculate that the gC IFN-γ binding activity
487 could also impact gene expression in T cells at later stages of T cell mediated
488 pathogenesis, such as the release of virus at the skin and during infection of T cells
489 from keratinocytes prior to secondary viremia[5, 6, 7].
490 We validated the enhancement of ICAM1 at the mRNA and protein level and showed
491 that ICAM1 interaction with LFA-1 was required for the increased T cell adhesion
492 observed in the presence of gC and IFN-γ compared to IFN-γ alone. Infection with VZV
493 expressing gC also led to enhancement of ICAM1 levels and T cell adhesion. This
494 enhancement resulted in a trend of higher VZV spread from HaCaT to Jurkat cells and,
495 especially, to PBMCs. It has been previously shown that VZV infected T cells express
496 higher levels of LFA-1, and it was speculated to facilitate migration[4]. The increased
497 level of LFA-1 could also facilitate VZV spread to keratinocytes through an
498 immunological synapse-like formation. Some viruses, including human
499 immunodeficiency virus (HIV) and herpes simplex virus type 1 (HSV-1) transform the
500 immunological synapse into a virological synapse to facilitate cell-to-cell spread[43, 44].
501 IFN-γ inhibits VZV replication in different cell types[34], even more efficiently than
502 IFN-α[33]. *In vivo*, IFN-γ and other cytokines secreted by VZV-specific CD4 T cells
503 reduce VZV pathogenesis during primary infection and upon reactivation[45, 46]. Several

other VZV genes inhibit IFN-γ function[47, 48, 49, 50]. Interestingly, VZV gC did not seem to reduce the antiviral activity of IFN-γ, which inhibited VZV replication in HaCaT cells irrespective of the presence of gC. Similarly, IFN-γ reduced the spread of the virus from HaCaT to Jurkat cells and PBMCs. However, the virus expressing gC spread better to Jurkat cells and PBMCs than the ΔgC virus, even in the presence of IFN-γ. Therefore, the presence of gC during infection conferred an advantage to infect both Jurkat cells and PBMCs. VZV gC also facilitates VZV spread between human keratinocytes in skin xenografted in SCID mice[21]. During infection of human skin, gC is highly expressed[51] and gC expression is higher in highly virulent viruses than in an attenuated vaccine strain[38, 52]. All these results highlight the role of gC as a virulence factor.

An interesting and unsolved question is how VZV gC induces biased signalling through IFNGR. Most viral IFN-binding proteins bind to the cytokine through its receptor-interacting site in order to block IFN activity. Our results suggest that VZV gC binds to IFN-γ through its GAG-binding domain, and this would allow interaction of the cytokine with IFNGR. Based on the already known biased agonists of IFNGR[15], we hypothesise that gC induces conformational changes on IFN-γ that lead to different interaction with IFNGR chains, followed by modifications of signalling pathways and differential gene expression. Alternatively, it is possible that gC may also bind and signal through another receptor that coordinates with IFNGR to mediate an altered signalling. To address these hypotheses, we are currently seeking to obtain the crystal structure of gC bound to IFN-γ. As a surface glycoprotein that is located on the virion surface, it is likely that gC binds directly to receptors on the cell surface, not only to IFNGR but to another cellular protein that influences IFN-γ activity. Our data with neutralising antibodies to IFNGR show that signalling through this receptor is required for gC enhancement of ICAM1 expression in epithelial cells. Moreover, although gC alone

enhanced the expression of few genes, the effect size was not large enough to result in observable phenotypic changes in ICAM1 protein levels and cell adhesion. Finally, $gC_{Y419\text{-}S523}$ bound IFN-γ only transiently and did not increase its activity, suggesting that stable interaction with the cytokine through residues Y322-S523 is required to enhance ICAM1 expression in several cell lines and T cell adhesion. Overall, these results suggest that gC activity requires high affinity interaction with IFN-γ and signalling through the IFNGR. However, gC increased ICAM1 protein independently of IFN-γ in human iPSC-derived macrophages, suggesting that gC can also act independently of IFN-γ in these cells. Moreover, VZV gC increased spread from HaCaT cells to PBMCs even without exogenous addition of IFN-γ. This could also point to the existence of an unknown interaction of gC with a receptor expressed on these cells. Alternatively, it could also be due to the presence of IFN-γ secreted by PBMCs. Overall, our results advance the knowledge in the field of viral immunomodulation by the discovery of a viral protein that binds and modulates IFN-γ activity, acting as the only yet known viral IFN-γ biased agonist, increasing the expression of few ISGs, including ICAM1 and leading to higher T cell adhesion and VZV spread to lymphocytes. This is highly relevant due to the importance of lymphocyte infection for VZV spread and pathogenesis. Moreover, IFN-γ-based therapies are complicated by the large number of ISGs induced and their pleiotropic activities. The information obtained here could serve to design specific IFN-γ agonists that have therapeutic potential, as previously suggested[15].

Materials and Methods

Ethic statement

Peripheral blood mononuclear cells (PBMCs) from anonymised healthy blood donors were provided from the Institute of Transfusion Medicine, MHH, Germany. The donors

signed a consent for the use of small amounts of their blood for research purposes, approved by the Ethics Committee of Hannover Medical School #2519-2014 and #10476_BO_K_2022.

Cytokines

Recombinant cytokines (IFN-α, IFN-β, IFN-γ, IFN-λ1, IFN-λ2, IFN-ω, and TNF-α) were purchased from PeproTech. The different IFN-α subtypes (IFN-α1, IFN-α2, IFN-α4, IFN-α5, IFN-α6, IFN-α7, IFN-α8, IFN-α10, IFN-α14, IFN-α16, IFN-α17, and IFN-α21) have been previously described[53] and kindly provided by Ulf Dittmer (University Hospital Essen)

Construct design

The coding sequences of different gC constructs were introduced into a pMT vector backbone[54] for expression in Drosophila S2 cells. The genes were inserted downstream a Drosophila BiP signal sequence to direct proteins to the endoplasmic reticulum and all constructs had a double strep-tag for efficient protein purification. All gC constructs were amplified from the VZV Dumas strain (Accession Number GenBank: X04370.1) using primers shown in Table 1. The $gC_{P23\text{-}V531}$ and $gC_{S147\text{-}V531}$ were cloned using a restriction enzyme-based strategy (*Bgl*II and *Spe*I sites) as described before[18]. The $gC_{P23\text{-}V531}$ resembles the His-tagged rSgC previously reported[18] while the $gC_{S147\text{-}V531}$ lacks the 7 N-terminal residues present in the previously reported IgD-Strep[18] based on bioinformatic analyses. To generate $gC_{Y322\text{-}S523}$ and $gC_{Y419\text{-}S523}$ we performed restriction-free cloning [55].

Oligo name	Sequence (5' to 3')
$gC_{P23\text{-}V531}$-forward	TAT**AGATCT**CCCACACCCGTAAGTATAACT
$gC_{S147\text{-}V531}$-forward	TAT**AGATCT**TCACAACCACCTTTTCTA

gC-reverse	TATTTA**ACTAGT**AACGGAAAATGTAGTGGC
$gC_{Y322\text{-}S523}$-forward	CTTTGTTGGCCTCTCGCTCGGGTATCGTCCAAATATTACCGTTGTCG
$gC_{Y419\text{-}S523}$-forward	CTTTGTTGGCCTCTCGCTCGGGTATTCTGCTGTCGTTACCCC
gC_{RFC}-reverse	CAACCGGCCTTATCGTCATCGTCAGATGCATCGTAGGTATAAACGG

Table 1: Oligonucleotides employed for cloning the different gC constructs. Restriction sites are indicated in bold.

Production of recombinant proteins

For expression and purification of the soluble gC constructs, stable S2 transfectants were established and proteins produced as described previously[56] with minor modifications. Briefly, 2-µg of gC expression plasmid was co-transfected with 0.1 µg pCoPuro plasmid[57]. Following a 6-day selection period with puromycin (8 µg/mL), stable cell lines were adapted and grown in insect-Xpress media (Lonza). For large-scale production, supernatant from cells incubated with 4 µM $CdCl_2$ for 5 days was collected and soluble protein was purified by affinity chromatography using a Strep-Tactin XT 4Flow column (IBA Lifesciences) followed by size exclusion chromatography using a HiLoad 26/600 superdex 200 pg column (Cytiva) equilibrated in 20 mM HEPES pH 7.4 and 150 mM NaCl at 2 mL/min flow rate. For cell culture assays, purified proteins were buffer exchanged to PBS using a superdex 200 increase 10/300 column (Cytiva) equilibrated with PBS at 0.5 mL/min flow rate. Protein purity was analyzed on Coomassie-stained SDS-PAGE gels or using stain-free TCE gels[58]. Fractions containing pure protein were concentrated, flash-frozen, and stored at -80 °C until required for further analysis.

Generation of recombinant VZV

Recombinant, BAC-derived pOka-ΔgC-GFP, pOka-gC-GFP and pOka-Δ57-GFP were employed in this study. pOka-ΔgC-GFP was described before[18] and contains an

enhanced monomeric GFP instead of *ORF14*. Recombinant VZV expressing gC-GFP protein (pOka-gC-GFP) was generated by *en passant* mutagenesis through addition of a 5 × alanine linker followed by monomeric enhanced GFP (GFP) to the 3' end of *ORF14* in the background of previously generated BAC-pOka strain[37, 59]. The BAC-pOka was mutated by insertion of 5 x Alanine linker-GFP-Kanamycin resistance (KanR) cassette in which an excisable KanR gene disrupts the GFP ORF. The KanR is flanked by a duplicated fragment of GFP sequence and I-*Sce*I restriction sites, which allows subsequent excision of KanR and the seamless repair of the GFP ORF by Red recombination in *E. coli* strain GS1783[37]. The cassettes were amplified by PCR with the plasmid pEP-GFP-in[60] as template and using the following primers to fuse the gC with the GFP gene in the BAC. Fwd 5'-TATCGCAGTTATCGCAACCCTATGCATCCGTTGCTGTTCAGCAGCAGCA GCAGCAATGGTGAGCAAGGGCGAGGA-3' and Rev-5'-AAAATGATATACACAGACGCGTTTGGTTGGTTTCTGTTTACTTGTACAGCTCG TCCATG-3'.

The recombinant pOkaDXRR57DG (here called pOka-Δ57-GFP) was developed by BAC mutagenesis using the pOka DXRR BAC recently published[61] that has corrections for two spurious mutations found in the original pOka BAC DX[59]. An mCherry Kan-in cassette with an internal *Isce*I was kindly provided by Dr Gregory Smith (Northwestern University Chicago, IL). Two oligos were used to create a new complete deletion of ORF57 and the insertion of the GFP-kan in gene: 57FF 5'-AAAATACTTTGACCGACCAACCAATTAATACTGAAAATAGCGGTC**ATG**GACGT ACGAGAACGTAAT*GTGAGCAAGGGCGAG*-3' and 57R 5'-GATTATATTTAACGGCTTTTAATTTGAAGACACCTATCCTCTG*ACATCACTTGT ACAGCTCGTCCAT*-3'. The design of the deletion primers was such that 18 nucleotides of the beginning of the ORF57 gene are retained (ORF57ATG in bold) as

a fusion to the fluorescent gene so that the deletion does not affect the small region of ORF58 C-terminus that overlaps ORF57 underlined. The sequence denoted in italics is that homologous to the fluorescent gene. The purified PCR amplified fragment was electroporated into bacterial strain GS1783 containing the pOka DXRR after the induction of the recombination enzymes, and recombination was selected by gain of kanamycin resistance as recently detailed by Lloyd et al., 2022[61] and previous publications from the Kinchington Laboratory.

Positive colonies were then grown, induced for I-*Sce*I expression by addition of Arabinose, and subjected to a heat induction to induce the λRec Recombination enzymes. Following plating on plates lacking kanamycin but containing Arabinose, colonies were then screened for loss of kanamycin resistance by replica plating. All BACs were verified for insertion into the correct site by RFLP analysis and sequencing across junctions.

To reconstitute infectious recombinant viruses, MeWo cells were transfected with fresh BAC DNA using Lipofectamine 2000 (Invitrogen) or TransIT-X2 (Mirus) in a 6-well plate (10 µl Lipofectamine + up to 100 µl of BAC-VZV DNA). Lipofectamine-DNA complexes were produced in OptiMEM and added onto subconfluent (~80%) MeWo cells in a dropwise manner. After 24 h medium was changed and cells were incubated with maintenance splits of cells every week until formation of syncytia.

Preparation of virus stocks

Non-infected cells were seeded the day prior to infection to about 75% confluency. For infection, an inoculation rate of one infected cell to 5-7 uninfected cells was used in media with 2% FBS. The cell-associated virus inoculum was left on the cells in case the same cell line was used for virus production. Otherwise, the inoculum was removed after 2 – 3 h and the cells were washed to remove any contaminating cell types.

Infected cells were frozen in medium with 20% FBS and 10% DMSO and used as inoculum after thawing and removal of the DMSO-containing freezing medium.

VZV replication kinetics

HaCaT cells were seeded one day prior to infection with a density of 9×10^4 cells/well of a 24-well plate. Cells were subconfluent for infection with 100 PFU/well in 250 µL infection medium (growth medium with only 2% heat-inactivated FCS) for 2 h at 37 °C, 5% CO2, in a humidified incubator. Inoculum was washed off and replaced by infection medium. Samples were harvested at 0, 10, 24, 48 and 72 hours post-infection by replacing the medium with 1× DPBS, followed by imaging at the Cytation3 (BioTek). Then, cells were detached using trypsin/EDTA, frozen in the respective growth medium described in the '"Cell culture" section, supplemented with 20% FCS and 10% DMSO, and stored at -80 °C until titration of the samples. Experiment was performed with triplicates.

End point dilution assays

End point dilution assays were performed to determine the tissue culture infectious dose 50 ($TCID_{50}$) values. HaCaT cells were used for titration of viruses. Cell-associated virus from HaCaT cells was thawed quickly in a 37 °C water bath, followed by washing with infection medium to remove DMSO. A 1:5 dilution series of the virus was prepared in infection medium, with at least 4 replicas per virus stock. The medium of HaCat cells was discarded and replaced by the diluted virus followed by incubation for 5 to 6 days. The infected wells per dilution step were counted and the $TCID_{50}$/mL and PFU/mL were calculated using the $TCID_{50}$ calculator provided online by Marco Binder (Dept. Infectious Diseases, Molecular Virology, Heidelberg University, Germany), which is

based on the Spearman & Kärber algorithm. The PFU/mL was calculated by multiplying the $TCID_{50}$/mL by 0.69.

Biophysical protein-protein interaction studies

Surface plasmon resonance (SPR)

The Biacore X100 and S200 systems were used to investigate protein-protein interactions by SPR. All experiments were performed with 1× HBS-EP as running buffer, if not stated otherwise, and at 25 °C. A pH scouting was performed to find optimal conditions of protein immobilisation. To do so, the protein was diluted at least 1:10 in sodium acetate buffer with different pH (4.5, 5 and 5.5) or maleate pH 5.9 and injected onto the chip surface, which was afterwards washed using 50 mM NaOH. Immobilisation was performed using the amine coupling kit and wizard according to the manufacturer's instructions, leading to covalent coupling of protein ligand on CM4 or CM5 chips. Depending on the purpose the target level was specified. Flow cell 1 (FC1) was always used as a negative control. For screening experiments and GAG competition assays, the association time was set to 90 s and the dissociation time was set to 60 s, and analytes were injected at a flow rate of 10 µL/min and a concentration of 100 nM. For GAG-competition assays the analyte was mixed with increasing amounts of the GAG (w:w ratio). For kinetics experiments, the association time was set to 90 s and the dissociation time was set to 420 s, and analytes were injected at a flow rate of 30 µL/min and in a concentration ranging from 0.39 nM to 50 nM. After each analyte injection, the surface was regenerated using 10 mM glycine pH 2. In each run 2 – 3 cycles with 1× HBS-EP were included as a control and for subtraction of the blank signal. Analysis and sensorgram adjustment were performed using the Biacore X100 or S200 Evaluation software. The FCx−FC1 was calculated, and a blank injection was subtracted to obtain the specific signal for the binding to the ligand.

704 Grating-coupled interferometry (GCI)

705 The Creoptix WAVEdelta system was used to investigate protein-protein interactions
706 by GCI. DXH chips were used to analyse the gC – IFN interaction. These chips have
707 a dextran surface similar to the CM4/5 chips from the Biacore system and can be used
708 for covalent immobilisation by amine coupling. In a first step, the chip was conditioned
709 with borate pH 9 to ensure a proper hydration of the surface. A pH-scouting was
710 performed to find optimal conditions for capture and immobilisation. Both, pH scouting
711 and immobilization were performed following a similar protocol as for the Biacore
712 system but using 0.2× HBS-EP (filtered and degassed) as running buffer and a specific
713 immobilization time, set according to the desired immobilisation level and based on the
714 response obtained during pH scouting. For kinetic experiments, the RAPID wizard for
715 tight binders (fr 50 µL/min, acq 1 Hz, ass 120 s, diss 1800 s) was used. As running
716 buffer for binding and kinetic experiments filtered and degassed 1× HBS-EP was used.
717

718 **Detection of ICAM1 and MHCII by flow cytometry**

719 Adherent cell lines were seeded (1×10^5 HaCaT, 2.5×10^5 MeWo and 0.625×10^5
720 A549 cells) a day in advance into 48-well plates and incubated for 18-24 h at 37 °C,
721 5% CO_2 in a humidified incubator. Jurkat cells were passaged 1:2 and the day of the
722 experiment 2×10^5 cells were seeded into 48-well plates. The iPSC-derived
723 macrophages were seeded at 0.15×10^6 cells/48-well and cultivated in RPMI1640
724 supplemented with 10% FCS, 1% Pen/Strep, and 50 ng/mL huM-CSF (Peprotech) for
725 4 days and then stimulated.
726 Stimulation mix containing IFN-γ, gC or both, was prepared in 1× DPBS and
727 preincubated for 30 min at 37 °C, then growth medium was added. The medium was
728 removed from the cells and the stimulation medium was added. To neutralize IFNGR
729 signalling, cells were incubated with 2 µg/mL IFNGR1-neutralizing antibody (BD

Bioscience #557531) or an isotype control (BD Bioscience #554721) for 2 h prior to stimulation. The stimulation mix was added to the antibody-containing medium. Stimulation of cell lines lasted 24 h while that of iPSC-derived macrophages was performed during 2, 5, 8, 12 and 24 h, both at 37 °C, 5% CO_2 in a humidified incubator. To analyse cells by flow cytometry, the cells were detached with accutase, washed twice with 1× DPBS + 1% FCS (and 2.5 mM Ca^{2+} if annexinV staining was included). Cells were kept on ice after detachment and stained for 30 min with anti-ICAM1-PE (Biolegend #353106) and anti-MHCII-FITC (ImmunoTools #21629233X2), and Zombie-NIR (Biolegend #423106). Afterwards, cells were washed again twice with DPBS + 1% FCS (and 2.5 mM Ca^{2+} for the first wash if annexinV was included) and resuspended in DPBS + 1% FCS for measurement at the Cytoflex. Macrophages were rinsed of at the end of the stimulation time and stained for flow cytometric analysis.

To determine ICAM1 levels during infection, 1 × 10^5 HaCaT cells were seeded into 12-well plates. The next day, cells were infected with 7.5 × 10^4 PFU HaCaT-associated VZV Δ57-GFP reporter virus in a volume of 500 µL infection medium for 2 h at 37 °C and 5% CO_2 in humidified incubator. Afterwards, the inoculum was removed, cells were washed with 1× DPBS, and fresh infection medium was added. Cells were further incubated for 2 days. Then, cells were stimulated with 5 ng/mL IFN-γ or mock treated for 24 h. Cells were detached using accutase and stained for 30 min with anti-ICAM1-APC (Biolegend #353111) and Zombie-NIR (Biolegend #423106). After the last washing step, cells were resuspended in 100 µL 4% PFA and incubated on ice for 15 min with mixing every 5 min. Then, cells were washed once more with DPBS + 1% FCS and resuspended for analysis at the Cytoflex. For analysis, first, the cell population was included, then doublets and dead cells were excluded. The remaining population was gated for a GFP^- = uninfected (or uninfected bystander in VZV inoculated cultures) population and a GFP^+ = productively infected population. Based

on the GFP levels, we further distinguished between a GFP^{high} and GFP^{low} population within the infected cells.

RNA Isolation

To isolate RNA, the NucleoSpin® RNA kit (Macherey and Nagel) was used for general purpose and RNAseq experiments in which cells were cultured in 6-well format. To isolate RNA from cells cultured in 96-well plates, the Quick-RNA™ MicroPrep kit from Zymo was used. Both kits were used according to the manufacturer's instructions. The RNA concentration was quantified photometrically using the NanoDrop 1000. RNA was stored at -80 °C or, if possible, directly processed to obtain cDNA as explained in the "RT-qPCR" section, below.

Acetone precipitation

Acetone precipitation was used to recover the proteins from samples used for RNA isolation according to the manufacturer's instructions of the RNA isolation kit (Quick-RNA™ Microprep Kit from Zymo). Therefore, 1 volume of the collected flow-through from RNA isolation was mixed with 4 volumes of pre-chilled acetone (-20 °C) and incubated at -20 °C for at least 30 min. Then, samples were centrifuged at 17,000 × g for 10 min and the SN discarded. The protein pellet was washed with ethanol and after another spin at 17,000 × g for 1 min and removal of the SN, the pellet was air-dried for 10 min at RT. Afterwards, the pellet was resuspended in 20 µL 5× SDS sample buffer with β-mercaptoethanol and subjected to SDS-PAGE and western blotting.

RT-qPCR

RT-qPCR was performed following a two-step protocol. For cDNA synthesis, the LunaScript® RT Super Mix Kit from NEB was used according to the manufacturer's

instructions. For qPCR analysis, the Luna® Universal qPCR Master Mix from NEB was used according to the manufacturer's instructions with a total reaction volume of 10 µL. For gene expression analysis, 1 ng RNA/cDNA was used as template and amplified with oligonucleotides shown in Table 2. The qTower^3 from Analytic Jena with the qPCRsoft 4.1 software was used. The ΔΔCt-method was used to analyse the data using the qPCRsoft 4.1 (Analytik Jena) Software following the Livak method. Actin was used for normalization.

Oligo name	Sequence (5' to 3')
Actin-fwd	CTTCGCGGGCGACGAT
Actin-rev	CCACATAGGAATCCTTCTGACC
ICAM1-fwd	GTATGAACTGAGCAATGTGCAAG
ICAM1-rev	GTTCCACCCGTTCTGGAGTC
CXCL8-fwd	ACTGAGAGTGATTGAGAGTGGAC
CXCL8-rev	AACCCTCTGCACCCAGTTTTC
CXCL9-fwd	GGTGTTCTTTTCCTCTTGGGC
CXCL9-rev	AACAGCGACCCTTTCTCACT
CXCL10-fwd	GTGGCATTCAAGGAGTACCTC
CXCL10-rev	TGATGGCCTTCGATTCTGGATT
CXCL11-fwd	GAGTGTGAAGGGCATGGCTA
CXCL11-rev	ACATGGGGAAGCCTTGAACA
IL4I1-fwd	GCCAAGACCCCTTCGAGAAAT
IL4I1-rev	CCGATCCTGTTATCTGCCTCC

Table 2: Oligonucleotides employed for qPCR

RNA-Seq

HaCaT cells were seeded at a density of 0.8 × 10^6 cells/well of a 6-well plate to obtain a confluent cell layer the next day. For stimulation, a 10× stimulation mix of IFN-γ and/or $gC_{S147\text{-}V531}$ was prepared in 1× DPBS and preincubated 30 min at 37 °C. The

795 medium was replaced by 1,350 µL growth medium and 150 µL 10× stimulant was
796 added for 4 h. The final concentrations of IFN-γ and $gC_{S147\text{-}V531}$ were 5 ng/mL and 300
797 nM, respectively. Incubation of the cells was performed in a humidified incubator at 37
798 °C and 5% CO_2. Afterwards, the RNA was isolated as described above. RNA quality
799 control was performed by the RCU Genomics using a 2100 Bioanalyzer (Agilent).
800 Library generation, quality control, and sequencing as well as BCL to FASTQ
801 conversion were performed by Novogene (Cambridge, UK). Briefly, mRNA was
802 purified from total RNA using poly-T oligo-attached magnetic beads. After
803 fragmentation, the first strand cDNA was synthesized using random hexamer primers,
804 followed by the second strand cDNA synthesis using dTTP for non-directional library
805 (NEB Next® Ultra RNA Library Prep Kit for Illumina®). After end repair, A-tailing,
806 adapter ligation, size selection, amplification, and purification, fragment length
807 distribution of individual libraries was monitored using an Agilent 2100 Bioanalyzer.
808 Quantification of libraries was performed by use of Qubit and real-time PCR.
809 Equimolar amounts of individually barcoded libraries were pooled for a paired-end 150
810 bp sequencing run on an Illumina NovaSeq6000 S4 (300 cycles). The clustering of the
811 index-coded samples was performed according to the manufacturer's instructions.
812 Raw reads of FASTQ format were firstly processed by Novogene and reads containing
813 adapters, poly-N, and low-quality nucleotides removed.
814 Raw data processing was conducted by use of nfcore/rnaseq (version 1.4.2; National
815 Genomics Infrastructure at SciLifeLab Stockholm, Sweden), using the bioinformatics
816 workflow tool Nextflow to pre-processes raw data from FastQ inputs, align the reads
817 and perform quality-control. The genome reference and annotation data were taken
818 from GENCODE.org (Homo sapiens: GRCh38.p13; release 34).
819 Quality control and processing of sequencing raw data (bulk RNA-seq experiment) was
820 conducted by the Research Core Unit Genomics (RCUG) at Hannover Medical School.

Normalization and differential expression analysis were performed on the internal Galaxy (version 20.05) with DESeq2 (Galaxy Tool Version 2.11.40.6) with default settings except for “Output normalized counts table”, which was set to “Yes” and all additional filters were disabled (“Turn off outliers replacement”, “Turn off outliers filtering”, and “Turn off independent filtering” set “Yes”). Analysis was performed with multiple levels of primary factor (all different stimulations conditions) comparing all levels against each other.

Rstudio and Excel were used to sort for interesting genes based on adjusted *P* values and fold changes. Additionally, Excel was used to calculate the effect sizes from the normalized gene counts and fold changes thereof.

RNAseq data has been deposited at GEO with the following accession number PRJEB61951

Cell adhesion and virus spread assays

Adhesion assay: 3 × 10^4 HaCaT cells were seeded into a 96-well plate to reach confluence for the next day. Then, Jurkat cells were split 1:2 and the HaCaT cells were stimulated with IFN-γ +/- recombinant gC at concentrations indicated in the respective figure legends (if not stated otherwise 5 ng/mL IFN-γ and 300 nM gC were used). The stimulants were prepared in 1× DPBS, preincubated for 30 min at 37 °C, then growth medium was incorporated and the mixture was added to the cells following removal of the old medium. Triplicates were prepared for each condition.

For adhesion on infected cells, 1.5 × 10^4 HaCaT cells were seeded per well of 96-well plates to obtain a subconfluent cell layer. The next day cells were incubated with 7.5 × 10^2 PFU of BAC-derived VZV pOka gC-GFP or ΔgC-GFP in infection medium for 2 h at 37 °C. Then, the inoculum was pipetted up and down and removed, followed by a washing step with 1× DPBS. Next, infection medium was added and the cells were

incubated in a humidified incubator at 37 °C and 5% CO_2. After 2 days, cells were stimulated with different concentrations of 0, 0.5 or 5 ng/mLIFN-γ (prepared as 10× in 1× DPBS and diluted in infection medium). Triplicates were prepared for each condition.

After 24 h of stimulation, Jurkat cells were loaded with 5 µg/mL Hoechst 33342 and resuspended in RPMI supplemented with bivalent cations (1 mM Ca^{2+} and 2 mM Mg^{2+} final concentration) to 1.5 × 10^5/85 µL. The HaCaT cells were washed two times with 1× DPBS. Then, 85 µL/well of labelled Jurkat cells was added and the plate was immediately incubated for 15 min at 150 rpm and 37 °C. Afterwards, the non-adhered cells were taken off and the remaining cells were washed four times with DPBS supplemented with bivalent cations (1 mM Ca^{2+} and 2 mM Mg^{2+} final concentration). Then, the adhered Jurkat cells were imaged at the Cytation3 (BioTek) with two non-overlapping images per well (DAPI channel). Nuclei were counted using the CellProfiler Pipeline.

Virus spread assay: 5 × 10^5 HaCaT cells were seeded per well of a 48-well plate to obtain a subconfluent cell layer. Cells were inculated 24 hours later with 2 × 10^3 PFU BAC-derived VZV pOka gC-GFP or ΔgC-GFP in infection medium during 2 h at 37 °C, 5% CO2 in a humidified incubator. Afterwards, the inoculum was pipetted up and down and removed, followed by a washing step with DPBS. Next, infection medium was added and the cells were incubated in a humidified incubator at 37 °C and 5% CO_2. 2 days later, the infected HaCaT cells were stimulated with 0, 0.5, or 5 ng/mL IFN-γ (300 µL/well) for one day. The day before the start of the co-culture, Jurkat cells were passaged 1:2, and PBMCs were thawed and cultivated for one day in RPMI supplemented with 10% heat-inactivated FCS, 1× L-glutamine, 1× sodium pyruvate and 1× Pen/Strep at a density of 2 × 10^6 cell/mL at 37 °C and 5% CO_2 in a humidified incubator.

Before starting the co-culture, Jurkat cells and PBMCs were labelled with Hoechst 33342. The final cell pellet was resuspended at a density of 5×10^5 cell/250 µL. The infected HaCaT cells were washed two times with 1× DPBS, 250 µL of labelled Jurkat cells or PBMCs were added, and the plate was immediately incubated for 15 min at 150 rpm and 37 °C. Afterwards the non-adhered cells were taken off and the remaining cells were washed carefully four times with 500 µL DPBS supplemented with bivalent cations (1 mM Ca^{2+} and 2 mM Mg^{2+} final concentration). Then, a 1:1 mix of DMEM supplemented with 2% heat-inactivated FCS, 1× L-glutamine, and 1× Pen/Strep and RPMI supplemented with 2 % FCS, 1× L-glutamine, and 1× Pen/Strep medium was added and the cells were co-cultured at 37 °C and 5% CO_2 in a humidified incubator for 24 – 48 h.

To analyse the spread of VZV to Jurkat and PBMCs, all cells of the co-culture were collected and analysed by flow cytometry using the Cytoflex. Therefore, the medium, wash solution and trypsin/EDTA-detached cells were collected in FACS tubes. Cells were washed twice with FACS buffer (1% heat-inactivated FCS and 2mM EDTA in 1× DPBS) and then the pellet was resuspended in 300 µL FACS buffer containing 2.7% PFA (1:2 mix FACS buffer:4% PFA) and incubated for at least 30 min on ice. Afterwards, the GFP and Hoechst signals were measured at the Cytoflex.

Statistical analysis.

Statistical analysis was performed using GraphPad Prism. The dispersion measures, as well as the type of performed tests are indicated in the Fig. legends. Significances are indicated in the figures as ns = not significant; * = P <0.033; ** = P <0.002; *** = P <0.001.

Acknowledgements:

We thank Beate Sodeik, Martin Messerle (Hannover Medical School, Germany) and Thomas Pietschmann (Twincore, Hannover, Germany) for providing HaCaT, Jurkat E6.1 and A549 cell lines, respectively. Our gratitude also goes to Carsten Münk (Heinrich-Heine University Düsseldorf, Germany), for providing the Jurkat LFA1-KO cells. We thank Kathrin Sutter and Ulf Dittmer (University Hospital Essen, Germany) for providing the different IFN-α subtypes and Edward Fitzgerald (Malvern Panalytical, Creoptix) and Anja Drescher (Cytiva, Biacore) for technical support. We are grateful to Nikolaus Osterrieder (Freie Universität Berlin, Germany, and Cornell University, USA) for the wt BAC-derived VZV pOka strain. We thank Britta Eiz-Vesper (Hannover Medical School, Germany) for providing the blood to isolate PBMCs and all blood donors who agreed to the use of small amounts of blood for research. We thank the Research Core Unit Genomics (RCUG) at Hannover Medical School for performing quality control and processing of sequencing raw data (bulk RNA-seq experiment).

This work was funded by the Deutsche Forschungsgemeinschaft (DFG, German Research Foundation) under Germany's Excellence Strategy - EXC 2155 - project number 390874280 (https://www.resist-cluster.de/en/); by the Deutsche Forschungsgemeinschaft (DFG, German Research Foundation) – SFB 900/3 – project number 158989968 to AV-B (TPB9) and TK (TPB10) (https://www.mh-hannover.de/sfb900.html) and by the Deutsche Forschungsgemeinschaft (DFG, German Research Foundation). CJ and GS were funded by the Deutsche Forschungsgemeinschaft (DFG, German Research Foundation) project number 405772731, grants VI 762/1-1 and KR 2880/4-1, and GS by the German Federal Ministry of Education and Science (BMBF) via the Research network University Medicine (NUM; projects “COVIM” (FKZ: 01KX2021). CJ, GS, SB, NPB were supported by the Hannover Biomedical Research School (HBRS) and the Center for

925 Infection Biology (ZIB). PRK was supported by NIH awards AI158510, P30-EY08098,
926 and unrestricted awards from the Research to Prevent Blindness Inc, NY, and the Eye
927 & Ear Foundation of Pittsburgh. Generation of the GMP line LiPSC-GR1.1 was
928 supported by the NIH Common Fund Regenerative Medicine Program. The NIH
929 Common Fund and the National Center for Advancing Translational Sciences
930 (NCATS) are joint stewards of the LiPSC-GR1.1 resource.

931

932

References:

1. Ku CC, Padilla JA, Grose C, Butcher EC, Arvin AM. Tropism of varicella-zoster virus for human tonsillar CD4(+) T lymphocytes that express activation, memory, and skin homing markers. *Journal of virology* **76**, 11425-11433 (2002).

2. Moffat JF, Stein MD, Kaneshima H, Arvin AM. Tropism of varicella-zoster virus for human CD4+ and CD8+ T lymphocytes and epidermal cells in SCID-hu mice. *Journal of virology* **69**, 5236-5242 (1995).

3. Abendroth A, Morrow G, Cunningham AL, Slobedman B. Varicella-zoster virus infection of human dendritic cells and transmission to T cells: implications for virus dissemination in the host. *Journal of virology* **75**, 6183-6192 (2001).

4. Sen N*, et al.* Single-cell mass cytometry analysis of human tonsil T cell remodeling by varicella zoster virus. *Cell reports* **8**, 633-645 (2014).

5. Ku CC, Zerboni L, Ito H, Graham BS, Wallace M, Arvin AM. Varicella-zoster virus transfer to skin by T Cells and modulation of viral replication by epidermal cell interferon-alpha. *The Journal of experimental medicine* **200**, 917-925 (2004).

6. Ku CC, Besser J, Abendroth A, Grose C, Arvin AM. Varicella-Zoster virus pathogenesis and immunobiology: new concepts emerging from investigations with the SCIDhu mouse model. *Journal of virology* **79**, 2651-2658 (2005).

7. Arvin AM*, et al.* Varicella-zoster virus T cell tropism and the pathogenesis of skin infection. *Curr Top Microbiol Immunol* **342**, 189-209 (2010).

8. Campbell JJ, Hedrick J, Zlotnik A, Siani MA, Thompson DA, Butcher EC. Chemokines and the arrest of lymphocytes rolling under flow conditions. *Science* **279**, 381-384 (1998).

9. Harjunpaa H, Llort Asens M, Guenther C, Fagerholm SC. Cell Adhesion Molecules and Their Roles and Regulation in the Immune and Tumor Microenvironment. *Front Immunol* **10**, 1078 (2019).

10. Smith A, Bracke M, Leitinger B, Porter JC, Hogg N. LFA-1-induced T cell migration on ICAM-1 involves regulation of MLCK-mediated attachment and ROCK-dependent detachment. *J Cell Sci* **116**, 3123-3133 (2003).

11. Grakoui A*, et al.* The immunological synapse: a molecular machine controlling T cell activation. *Science* **285**, 221-227 (1999).

12. Andersen MH, Schrama D, Thor Straten P, Becker JC. Cytotoxic T cells. *J Invest Dermatol* **126**, 32-41 (2006).

13. de la Roche M, Asano Y, Griffiths GM. Origins of the cytolytic synapse. *Nat Rev Immunol* **16**, 421-432 (2016).

14. Schoggins JW. Interferon-Stimulated Genes: What Do They All Do? *Annu Rev Virol* **6**, 567-584 (2019).

15. Mendoza JL*, et al.* Structure of the IFNgamma receptor complex guides design of biased agonists. *Nature* **567**, 56-60 (2019).

16. González-Motos V, Kropp K, Viejo-Borbolla A. Chemokine binding proteins: An immunomodulatory strategy going viral. *Cytokine & Growth Factor Reviews*, (2016).

17. Heidarieh H, Hernaez B, Alcami A. Immune modulation by virus-encoded secreted chemokine binding proteins. *Virus research*, (2015).

18. Gonzalez-Motos V*, et al.* Varicella zoster virus glycoprotein C increases chemokine-mediated leukocyte migration. *PLoS Pathog* **13**, e1006346 (2017).

19. Viejo-Borbolla A*, et al.* Enhancement of chemokine function as an immunomodulatory strategy employed by human herpesviruses. *PLoS Pathog* **8**, e1002497 (2012).

20. Martinez-Martin N*, et al.* Herpes simplex virus enhances chemokine function through modulation of receptor trafficking and oligomerization. *Nat Commun* **6**, 6163 (2015).

21. Moffat JF, Zerboni L, Kinchington PR, Grose C, Kaneshima H, Arvin AM. Attenuation of the vaccine Oka strain of varicella-zoster virus and role of glycoprotein C in alphaherpesvirus virulence demonstrated in the SCID-hu mouse. *Journal of virology* **72**, 965-974 (1998).

22. Alcami A. Viral mimicry of cytokines, chemokines and their receptors. *Nat Rev Immunol* **3**, 36-50 (2003).

23. Huang J*, et al.* Inhibition of type I and type III interferons by a secreted glycoprotein from Yaba-like disease virus. *Proc Natl Acad Sci U S A* **104**, 9822-9827 (2007).

24. Montanuy I, Alejo A, Alcami A. Glycosaminoglycans mediate retention of the poxvirus type I interferon binding protein at the cell surface to locally block interferon antiviral responses. *FASEB J* **25**, 1960-1971 (2011).

25. Hernaez B*, et al.* A virus-encoded type I interferon decoy receptor enables evasion of host immunity through cell-surface binding. *Nat Commun* **9**, 5440 (2018).

1018 26. Alcami A, Symons JA, Smith GL. The vaccinia virus soluble alpha/beta interferon (IFN)
1019 receptor binds to the cell surface and protects cells from the antiviral effects of IFN. *Journal*
1020 *of virology* **74**, 11230-11239 (2000).

1021
1022 27. Qi F*, et al.* E3 ubiquitin ligase NEURL3 promotes innate antiviral response through catalyzing
1023 K63-linked ubiquitination of IRF7. *FASEB J* **36**, e22409 (2022).

1024
1025 28. Aubatin A, Sako N, Decrouy X, Donnadieu E, Molinier-Frenkel V, Castellano F. IL4-induced
1026 gene 1 is secreted at the immune synapse and modulates TCR activation independently of its
1027 enzymatic activity. *Eur J Immunol* **48**, 106-119 (2018).

1028
1029 29. Redondo M*, et al.* Differential expression of MHC class II genes in lung tumour cell lines. *Eur J*
1030 *Immunogenet* **25**, 385-391 (1998).

1031
1032 30. Holling TM, Schooten E, Langerak AW, van den Elsen PJ. Regulation of MHC class II
1033 expression in human T-cell malignancies. *Blood* **103**, 1438-1444 (2004).

1034
1035 31. Sheehan KC, Calderon J, Schreiber RD. Generation and characterization of monoclonal
1036 antibodies specific for the human IFN-gamma receptor. *J Immunol* **140**, 4231-4237 (1988).

1037
1038 32. Haake K*, et al.* Patient iPSC-Derived Macrophages to Study Inborn Errors of the IFN-gamma
1039 Responsive Pathway. *Cells* **9**, (2020).

1040
1041 33. Sen N, Sung P, Panda A, Arvin AM. Distinctive Roles for Type I and Type II Interferons and
1042 Interferon Regulatory Factors in the Host Cell Defense against Varicella-Zoster Virus. *Journal*
1043 *of virology* **92**, (2018).

1044
1045 34. Shakya AK, O'Callaghan DJ, Kim SK. Interferon Gamma Inhibits Varicella-Zoster Virus
1046 Replication in a Cell Line-Dependent Manner. *Journal of virology* **93**, (2019).

1047
1048 35. El Mjiyad N*, et al.* Varicella-zoster virus modulates NF-kappaB recruitment on selected
1049 cellular promoters. *Journal of virology* **81**, 13092-13104 (2007).

1050
1051 36. Nikkels AF, Sadzot-Delvaux C, Pierard GE. Absence of intercellular adhesion molecule 1
1052 expression in varicella zoster virus-infected keratinocytes during herpes zoster: another
1053 immune evasion strategy? *Am J Dermatopathol* **26**, 27-32 (2004).

1054
1055 37. Tischer BK, Smith GA, Osterrieder N. En passant mutagenesis: a two step markerless red
1056 recombination system. *Methods Mol Biol* **634**, 421-430 (2010).

1057
1058 38. Cohen JI, Seidel KE. Absence of varicella-zoster virus (VZV) glycoprotein V does not alter
1059 growth of VZV in vitro or sensitivity to heparin. *J Gen Virol* **75 (Pt 11)**, 3087-3093 (1994).

1060

39. Hernaez B, Alcami A. Virus-encoded cytokine and chemokine decoy receptors. *Curr Opin Immunol* **66**, 50-56 (2020).

40. Epperson ML, Lee CA, Fremont DH. Subversion of cytokine networks by virally encoded decoy receptors. *Immunol Rev* **250**, 199-215 (2012).

41. Lawson C, Wolf S. ICAM-1 signaling in endothelial cells. *Pharmacol Rep* **61**, 22-32 (2009).

42. Verma NK, Kelleher D. Not Just an Adhesion Molecule: LFA-1 Contact Tunes the T Lymphocyte Program. *J Immunol* **199**, 1213-1221 (2017).

43. Real F, Sennepin A, Ganor Y, Schmitt A, Bomsel M. Live Imaging of HIV-1 Transfer across T Cell Virological Synapse to Epithelial Cells that Promotes Stromal Macrophage Infection. *Cell reports* **23**, 1794-1805 (2018).

44. Aubert M, Yoon M, Sloan DD, Spear PG, Jerome KR. The virological synapse facilitates herpes simplex virus entry into T cells. *Journal of virology* **83**, 6171-6183 (2009).

45. Arvin AM, Koropchak CM, Williams BR, Grumet FC, Foung SK. Early immune response in healthy and immunocompromised subjects with primary varicella-zoster virus infection. *J Infect Dis* **154**, 422-429 (1986).

46. Weinberg A, Levin MJ. VZV T cell-mediated immunity. *Curr Top Microbiol Immunol* **342**, 341-357 (2010).

47. Abendroth A, Slobedman B, Springer ML, Blau HM, Arvin AM. Analysis of immune responses to varicella zoster viral proteins induced by DNA vaccination. *Antiviral Res* **44**, 179-192 (1999).

48. Abendroth A, Slobedman B, Lee E, Mellins E, Wallace M, Arvin AM. Modulation of major histocompatibility class II protein expression by varicella-zoster virus. *Journal of virology* **74**, 1900-1907 (2000).

49. Black AP, Jones L, Malavige GN, Ogg GS. Immune evasion during varicella zoster virus infection of keratinocytes. *Clin Exp Dermatol* **34**, e941-944 (2009).

50. Schaap A*, et al.* T-cell tropism and the role of ORF66 protein in pathogenesis of varicella-zoster virus infection. *Journal of virology* **79**, 12921-12933 (2005).

51. Storlie J, Carpenter JE, Jackson W, Grose C. Discordant varicella-zoster virus glycoprotein C expression and localization between cultured cells and human skin vesicles. *Virology* **382**, 171-181 (2008).

52. Kinchington PR, Ling P, Pensiero M, Moss B, Ruyechan WT, Hay J. The glycoprotein products of varicella-zoster virus gene 14 and their defective accumulation in a vaccine strain (Oka). *Journal of virology* **64**, 4540-4548 (1990).

53. Passos V*, et al.* Characterization of Endogenous SERINC5 Protein as Anti-HIV-1 Factor. *Journal of virology* **93**, (2019).

54. Krey T*, et al.* The disulfide bonds in glycoprotein E2 of hepatitis C virus reveal the tertiary organization of the molecule. *PLoS Pathog* **6**, e1000762 (2010).

55. Bond SR, Naus CC. RF-Cloning.org: an online tool for the design of restriction-free cloning projects. *Nucleic Acids Res* **40**, W209-213 (2012).

56. Backovic M, Krey T. Stable Drosophila Cell Lines: An Alternative Approach to Exogenous Protein Expression. *Methods Mol Biol* **1350**, 349-358 (2016).

57. Iwaki T, Figuera M, Ploplis VA, Castellino FJ. Rapid selection of Drosophila S2 cells with the puromycin resistance gene. *Biotechniques* **35**, 482-484, 486 (2003).

58. Ladner CL, Yang J, Turner RJ, Edwards RA. Visible fluorescent detection of proteins in polyacrylamide gels without staining. *Anal Biochem* **326**, 13-20 (2004).

59. Tischer BK, Kaufer BB, Sommer M, Wussow F, Arvin AM, Osterrieder N. A self-excisable infectious bacterial artificial chromosome clone of varicella-zoster virus allows analysis of the essential tegument protein encoded by ORF9. *Journal of virology* **81**, 13200-13208 (2007).

60. Sandbaumhuter M*, et al.* Cytosolic herpes simplex virus capsids not only require binding inner tegument protein pUL36 but also pUL37 for active transport prior to secondary envelopment. *Cell Microbiol* **15**, 248-269 (2013).

61. Lloyd MG*, et al.* Development of Robust Varicella Zoster Virus Luciferase Reporter Viruses for In Vivo Monitoring of Virus Growth and Its Antiviral Inhibition in Culture, Skin, and Humanized Mice. *Viruses* **14**, (2022).

Figure legends:

Figure 1. VZV gC binds type II IFN. (A) Schematic representation of VZV gC (top) and recombinant soluble gC constructs that were used in this study (below). All constructs contain a BiP signal peptide at the N-terminus and a Twin-Strep-tag. The first and last gC residue is indicated in each construct. The numbering of amino acid residues corresponds to the sequence of the Dumas strain. Abbreviations: AA = amino acid, SP = signal peptide, ECD = extracellular domain, TM = transmembrane domain, CD = cytoplasmic domain, R2 = repeated domain 2, IgD = immunoglobulin-like domain, BiP = Drosophila immunoglobulin binding chaperone protein signal sequence, Strep = Twin-Strep-tag with enterokinase site for optional removal of tag. **(B)** Sensorgram showing the results of a binding screening between VZV gC and cytokines using the Biacore X100 system. Recombinant purified VZV $gC_{P23\text{-}V531}$ was immobilized on a CM5 chip (3,600 RU). IFNs and TNFα were injected at 100 nM with a flow rate of 10 µL/min. Abbreviations: s = seconds, RU = resonance units.

Figure 2. VZV gC induces biased IFN-γ-induced gene expression. HaCaT cells were stimulated with IFN-γ, $gC_{S147\text{-}V531}$, both or mock treated for 4 h. RNA was isolated and further processed for RNAseq. **(A)** Venn diagram showing the number of genes, whose expression was modified in a statistically significant manner (*P* value < 0.05) for the three depicted comparisons. Differential gene expression analysis was performed comparing the different treatment conditions. **(B)** Normalized counts of genes with an adjusted (adj.) *P* value < 0.05 for either the comparison 'gC vs. mock' or 'both vs. IFN-γ' were plotted as heatmap after calculating the log2 and normalising (mean = 0, variance = 1) using Qlucore Omics Explorer 3.8. Hierarchical clustering was applied to sort for genes with a similar behaviour among the treatment conditions. Genes were classified in four different groups based on their expression change upon

stimulation with IFN-γ, gC or both. **(C-F)** Genes with an adj. *P* value < 0.05 for either the comparison 'gC vs. mock' or 'both vs. IFN-γ' were sorted into the four groups identified in the heatmap and the effect sizes were calculated and plotted. Arrows indicate genes that show more than a 1.5-fold change in their effect sizes between both comparisons. The coloured lines below the graphs indicate which genes were significantly regulated by IFN-γ alone. Striped bars indicate that the respective effect size was calculated from a not statistically significant regulated gene in that specific comparison. Panel (C) shows the genes regulated by IFN-γ and enhanced by gC. Panel (D) shows genes that were regulated when both were present. Panel (E) depicts genes mainly upregulated by gC alone and panel (F) includes genes that were upregulated by gC and weakened by IFN-γ.

Figure 3. gC enhances IFN-γ-induced ICAM1 and MHCII protein levels at the plasma membrane via IFNGR. (A, B) HaCaT cells were mock-stimulated or stimulated with 5 ng/mL IFN-γ, 300 nM VZV gC constructs or both for 24 h and then labelled with antibodies binding ICAM1, MHCII, and stained with Zombie-NIR dye. Cells were analysed by flow cytometry and median fluorescence intensities were determined after gating on single alive cells. Bar charts show the fold-change of ICAM1 (A) or MHCII (B) surface protein levels induced by gC constructs to either unstimulated or IFN-γ baseline. **(C, D)** HaCaT cells were pre-treated with 2 µg/mL IFNGR1-neutralizing antibody or isotype control for 2 h followed by mock-stimulation or stimulation with 5 ng/mL IFN-γ, 300 nM gC or both in the presence of neutralizing antibody or isotype control for 24 h and labelled with antibodies detecting ICAM1, MHCII, and stained with Zombie-NIR dye. Cells were analysed by flow cytometry and median fluorescence intensities were determined after gating on alive single cells. Bar charts showing the fold change of ICAM1 (C) or MHCII (D) levels compared to

unstimulated cells. One-way ANOVA, followed by Šídák's multiple comparisons was performed (comparing condition with gC to baseline without gC (A, B) and comparing between isotype and neutralizing antibody (C, D)). Non-significant comparisons are not depicted. * = P <0.033; ** = P <0.002; *** = P <0.001.

Figure 4. Co-stimulation of HaCaT cells with IFN-γ and gC increases adhesion of Jurkat cells. (A) Schematic representation of the assay. HaCaT cells were seeded one day prior to mock-stimulation or stimulation with IFN-γ, gC or both. 24 h after stimulation, Hoechst-labelled Jurkat cells were added and allowed to adhere during 15 min at 37 °C with shaking at 150 rpm. Then, non-adhered cells were washed off and two randomly selected regions of interest (ROI) were imaged per well (triplicate per condition) using an automated microscope (Cytation3, BioTek). The nuclei from adhered cells were quantified using a CellProfiler pipeline. **(B-D)** Adhered Jurkat cells per ROI plotted in a bar chart after normalization to the overall mean of adhered cells from each assay. Depicted are the comparisons between the four treatment conditions (B), the titration of the gC concentration (C), and the comparison of the different gC constructs (D). If not stated otherwise, 5 ng/mL IFN-γ and 300 nM gC were used. Shown is the mean ± SD. Filled circles represent the values from each independent assay (n=3). Ordinary one-way ANOVA followed by Šídák's multiple comparisons test (B, to test for preselected pairs) or followed by Dunnett's multiple comparisons test (C and D, to test each against a control = IFN-γ) were performed. **(E)** Adhesion assay comparing wild type (WT) Jurkat cells to LFA-1 KO Jurkat cells. Adhered cells per ROI are plotted in a bar chart. Shown is the mean ± SD. Filled circles represent the mean values from each independent assay (n=3, performed in triplicates with 2 ROI per well). Two-way ANOVA followed by Šídák's multiple comparisons test (to test between the

two cell types) was performed. ns = not significant; * = *P* <0.033; ** = *P* <0.002; *** = *P* <0.001.

Figure 5. Jurkat cells adhere better to cells infected with VZV-gC-GFP virus than with VZV-ΔgC-GFP. (A) Schematic representation of the assay. HaCaT cells were seeded 24 h prior to infection with VZV pOka expressing GFP fused to gC (gC-GFP) or expressing GFP instead of gC (ΔgC-GFP). 48 h after infection, the cells were stimulated with IFN-γ or mock-treated. The next day, Hoechst-labelled Jurkat cells were added and allowed to adhere during 15 min at 37 °C on a shaking platform at 150 rpm. Then, non-adhered cells were washed off and two randomly selected regions of interest (ROI) were imaged per well (triplicate per condition) using an automated microscope (Cytation3, BioTek) and the mean Hoechst and GFP intensities were determined. **(B-D)** Each circle corresponds to one experiment. Shown are the mean ± SD of the independent experiments. **(B)** Graph showing mean GFP fluorescence intensity obtained from HaCaT cells infected with VZV-gC-GFP or VZV-ΔgC-GFP and incubated or not with IFN-γ. **(C)** Bar chart showing the amount of adhered Jurkat cells normalised to the amount of infected HaCaT cells (Hoechst/GFP ratio) in the presence or absence of IFN-γ. **(D)** Graph showing the Hoechst/GFP ratio from HaCaT cells infected with VZV-gC-GFP divided by that of HaCaT cells infected with VZV-ΔgC-GFP and normalised to the mock-treated condition. Ordinary one-way ANOVA followed by Dunnett's multiple comparisons test (to test each against a control = no IFN-γ). ns = not significant; * = *P* <0.033; ** = *P* <0.002; *** = *P* <0.001. **(E)** Representative fluorescence microscopy images of Jurkat and HaCaT cells in the four experimental conditions. The GFP signal corresponding to productive infection is depicted in green, whereas the adhered Hoechst positive cells are shown in red.

Figure 6. VZV-gC-GFP spreads more efficiently from HaCaT cells to lymphocytes than VZV-ΔgC-GFP. Quantification of infected HaCaT, Jurkat cells and PBMCs by flow cytometry. Magenta indicates cultures infected with VZV-gC-GFP, grey indicates VZV-ΔgC-GFP infected cultures. **(A, B)** Percentages of GFP^+ HaCaT cells (A) and GFP^+ Jurkat cells (B) after co-culture are plotted as bar charts. **(C)** Ratio of GFP^+ Jurkat cells to GFP^+ HaCaT cells is plotted as bar chart. **(D)** The fold change attributed to the presence of gC is plotted as bar chart. **(E, F)** Percentages of GFP+ HaCaT cells (E) and GFP+ PBMCs (F) after co-culture are plotted as bar charts. **(G)** Ratio of GFP+ PBMCs to GFP+ HaCaT cells is plotted as bar chart. **(H)** The fold change attributed to the presence of gC is plotted as bar chart. Two-way ANOVA followed by Šídák's multiple comparisons test (to test between the two viruses) was performed. ns = not significant; * = P <0.033; ** = P <0.002; *** = P <0.001.

Figure 1

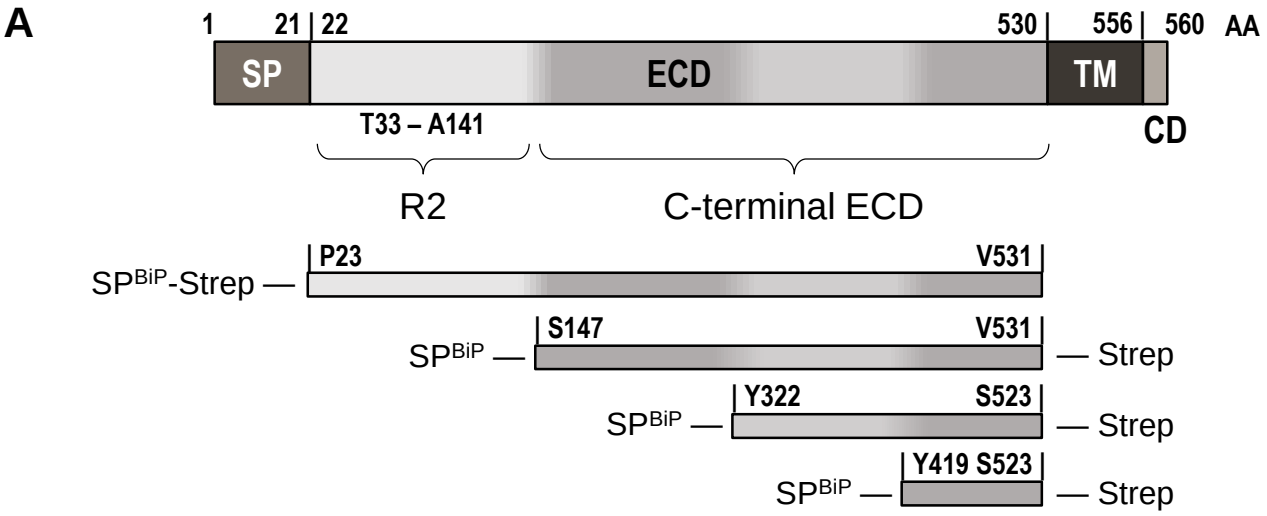
A
1
21
22
530
556
560
AA
SP
ECD
TM
CD
T33 – A141
R2
C-terminal ECD
SPBiP-Strep
P23
V531
SPBiP
S147
V531
Strep
SPBiP
Y322
S523
Strep
SPBiP
Y419 S523
Strep

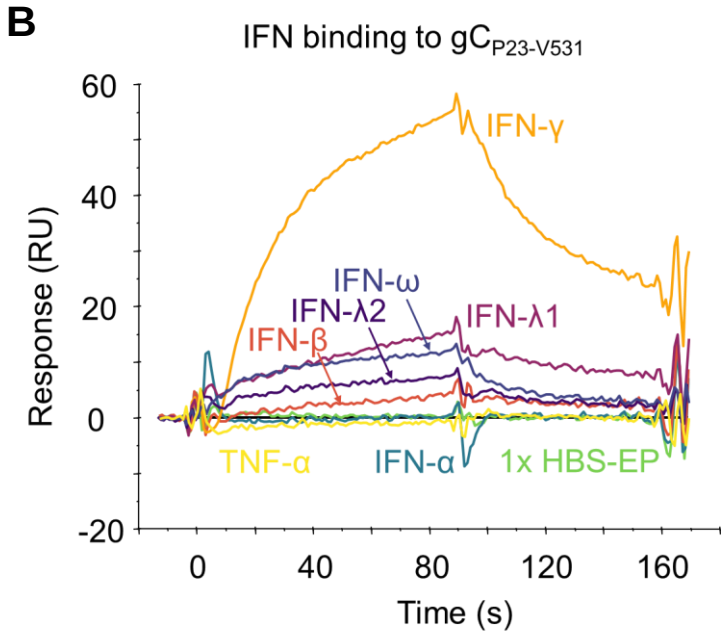
B
IFN binding to gCP23-V531
Response (RU)
60
40
20
0
-20
0
40
80
120
160
Time (s)
IFN-γ
IFN-ω
IFN-λ2
IFN-λ1
IFN-β
TNF-α
IFN-α
1x HBS-EP

Figure 2

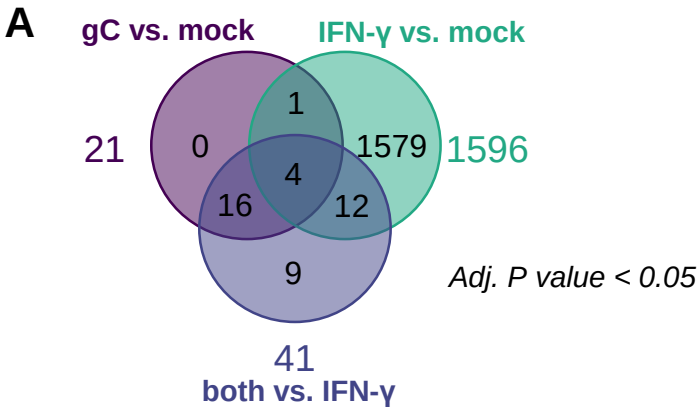
A
gC vs. mock
IFN-γ vs. mock
21
0
1
1579
1596
4
16
12
9
Adj. P value < 0.05
41
both vs. IFN-γ

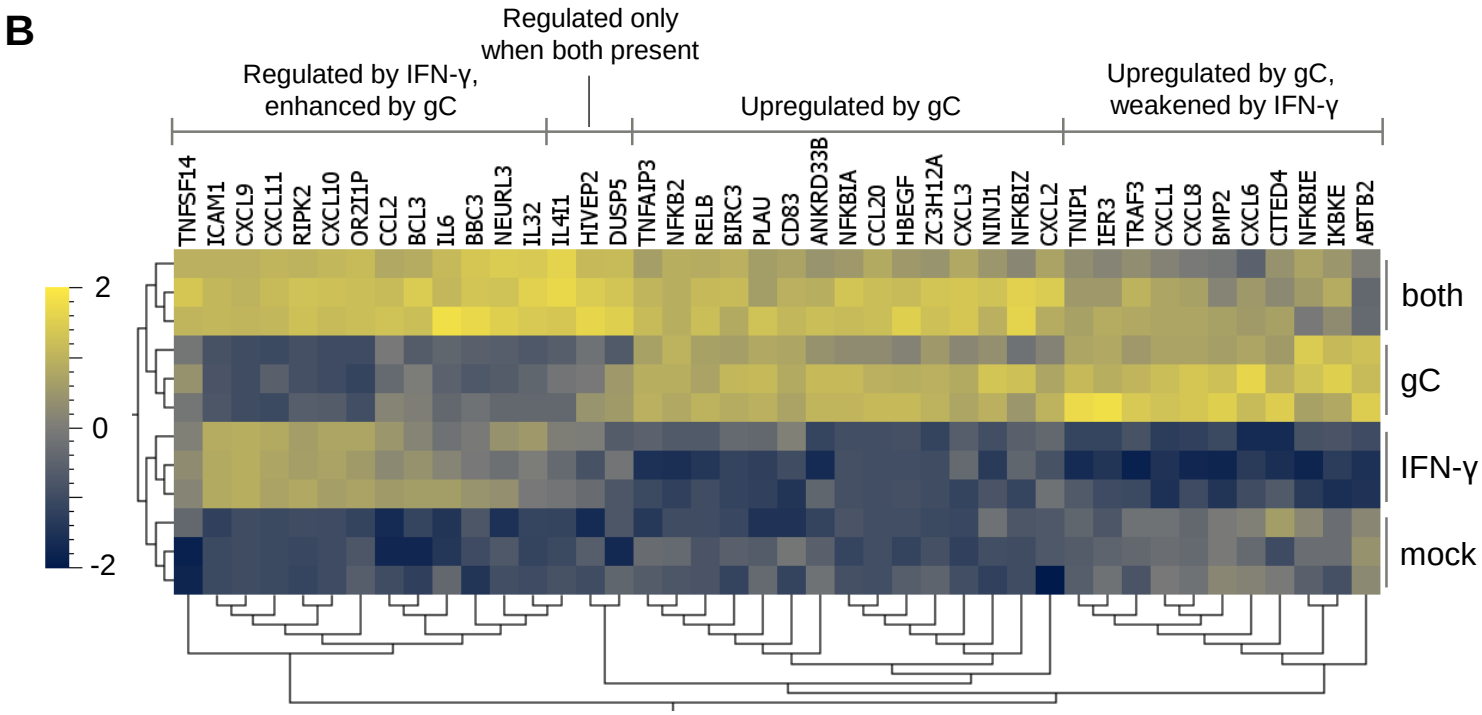
B
Regulated only when both present
Regulated by IFN-γ, enhanced by gC
Upregulated by gC
Upregulated by gC, weakened by IFN-γ
TNFSF14 ICAM1 CXCL9 CXCL11 RIPK2 CXCL10 OR2I1P CCL2 BCL3 IL6 BBC3 NEURL3 IL32 IL4I1 HIVEP2 DUSP5 TNFAIP3 NFKB2 RELB BIRC3 PLAU CD83 ANKRD33B NFKBIA CCL20 HBEGF ZC3H12A CXCL3 NINJ1 NFKBIZ CXCL2 TNIP1 IER3 TRAF3 CXCL1 CXCL8 BMP2 CXCL6 CITED4 NFKBIE IKBKE ABTB2
2
0
-2
both
gC
IFN-γ
mock

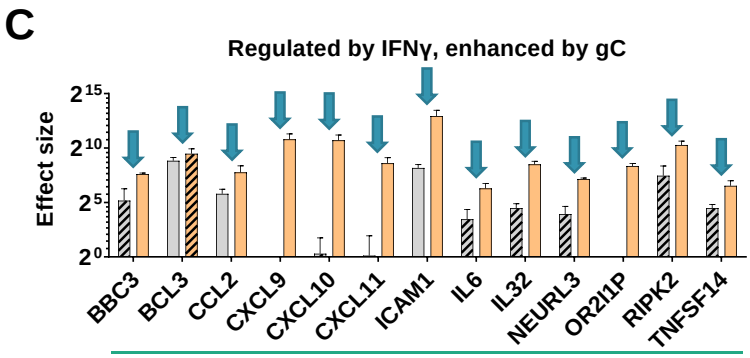
C
Regulated by IFNγ, enhanced by gC
Effect size
BBC3 BCL3 CCL2 CXCL9 CXCL10 CXCL11 ICAM1 IL6 IL32 NEURL3 OR2I1P RIPK2 TNFSF14

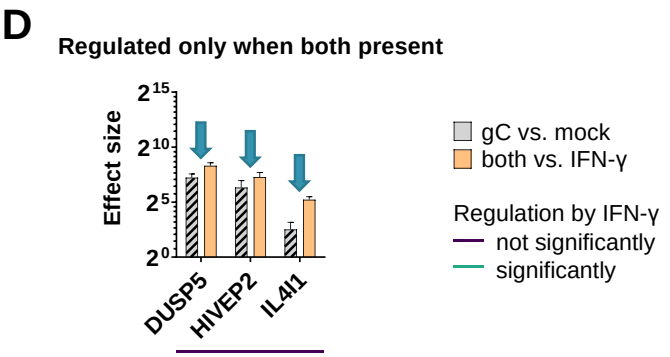
D
Regulated only when both present
Effect size
DUSP5 HIVEP2 IL4I1
gC vs. mock
both vs. IFN-γ
Regulation by IFN-γ
not significantly
significantly

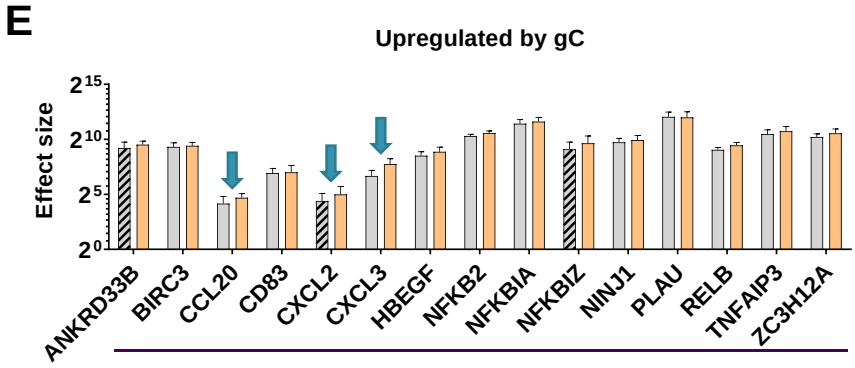
E
Upregulated by gC
Effect size
ANKRD33B BIRC3 CCL20 CD83 CXCL2 CXCL3 HBEGF NFKB2 NFKBIA NFKBIZ NINJ1 PLAU RELB TNFAIP3 ZC3H12A

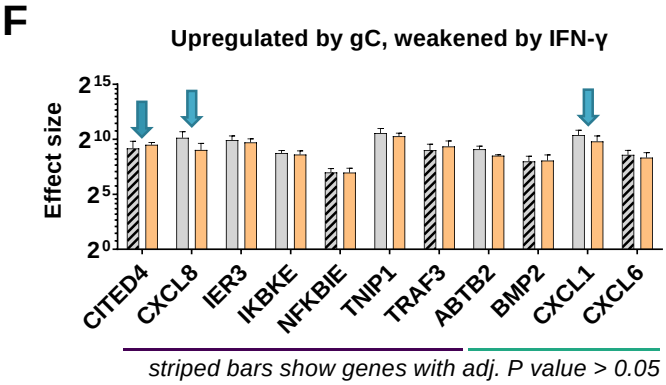
F
Upregulated by gC, weakened by IFN-γ
Effect size
CITED4 CXCL8 IER3 IKBKE NFKBIE TNIP1 TRAF3 ABTB2 BMP2 CXCL1 CXCL6
striped bars show genes with adj. P value > 0.05

Figure 3

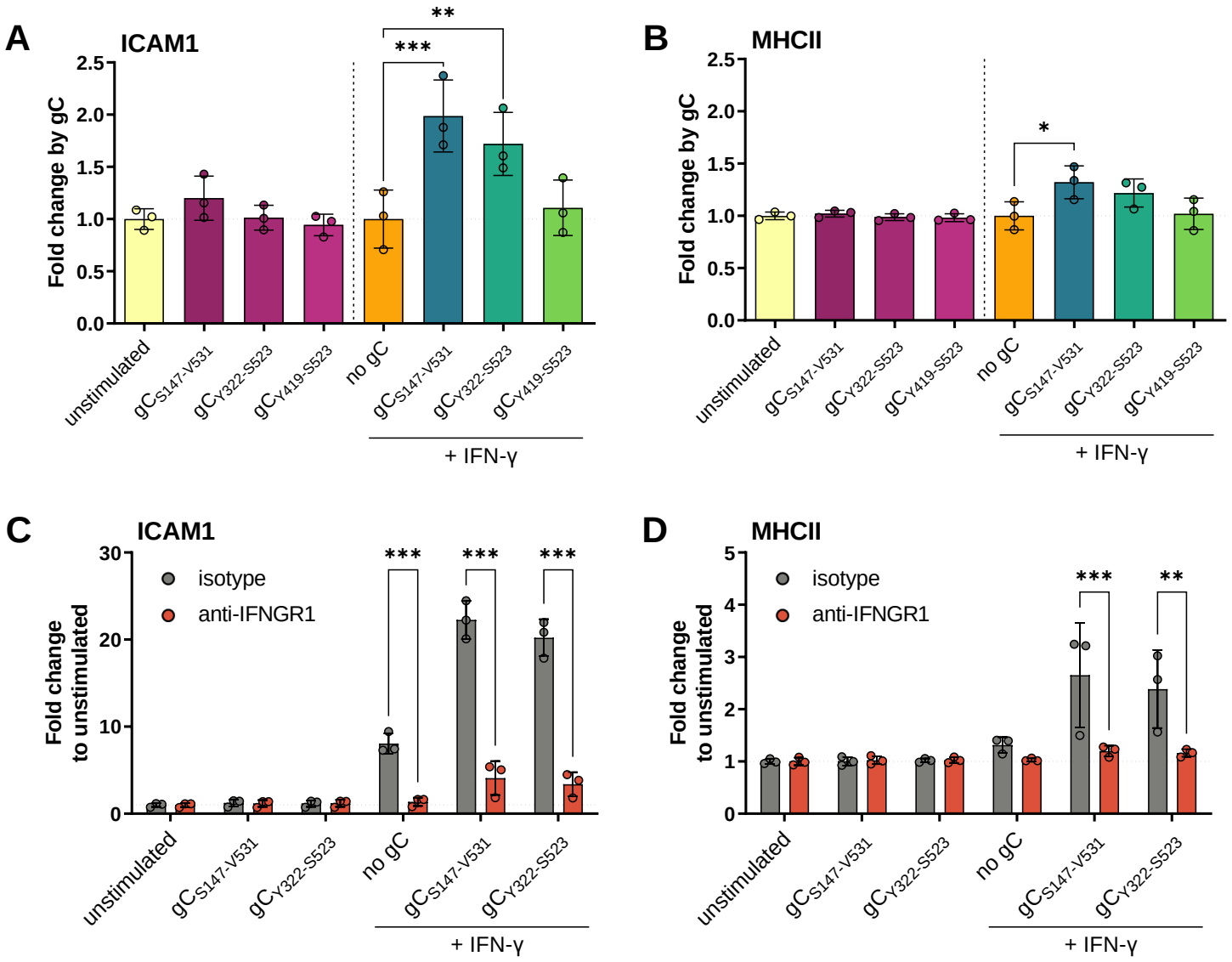
A
ICAM1
Fold change by gC
2.5
2.0
1.5
1.0
0.5
0.0
**
***
unstimulated
gCS147-V531
gCY322-S523
gCY419-S523
no gC
gCS147-V531
gCY322-S523
gCY419-S523
+ IFN-γ
B
MHCII
Fold change by gC
*
unstimulated
gCS147-V531
gCY322-S523
gCY419-S523
no gC
gCS147-V531
gCY322-S523
gCY419-S523
+ IFN-γ
C
ICAM1
Fold change to unstimulated
30
20
10
0
isotype
anti-IFNGR1
***
***
***
unstimulated
gCS147-V531
gCY322-S523
no gC
gCS147-V531
gCY322-S523
+ IFN-γ
D
MHCII
Fold change to unstimulated
5
4
3
2
1
0
isotype
anti-IFNGR1
***
**
unstimulated
gCS147-V531
gCY322-S523
no gC
gCS147-V531
gCY322-S523
+ IFN-γ

Figure 4

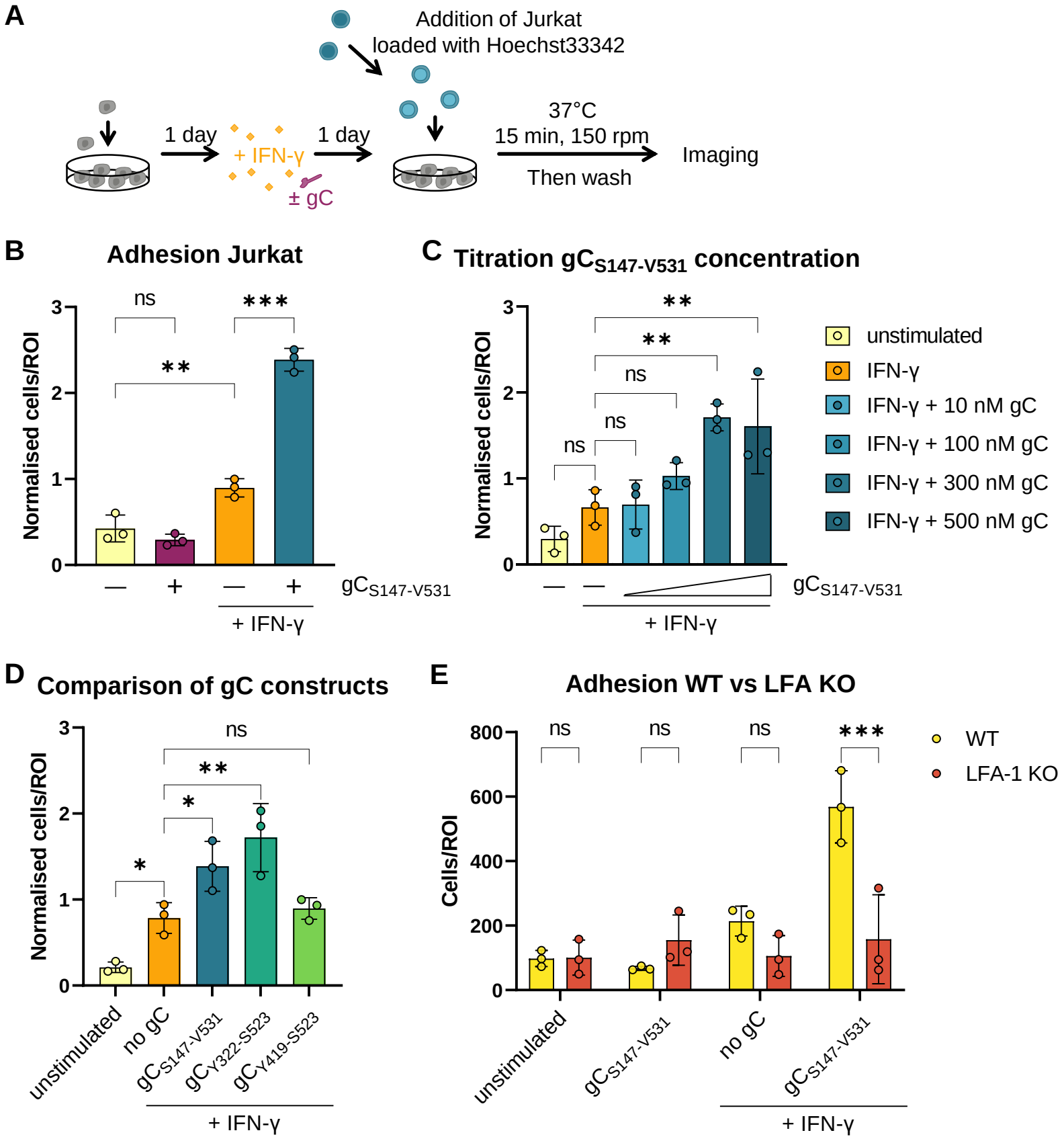
A
Addition of Jurkat
loaded with Hoechst33342
1 day
+ IFN-γ
± gC
1 day
37°C
15 min, 150 rpm
Then wash
Imaging
B
Adhesion Jurkat
Normalised cells/ROI
ns
***
**
—
+
—
+
gC S147-V531
+ IFN-γ
C
Titration gC S147-V531 concentration
Normalised cells/ROI
**
**
ns
ns
ns
unstimulated
IFN-γ
IFN-γ + 10 nM gC
IFN-γ + 100 nM gC
IFN-γ + 300 nM gC
IFN-γ + 500 nM gC
gC S147-V531
+ IFN-γ
D
Comparison of gC constructs
Normalised cells/ROI
ns
**
*
*
unstimulated
no gC
gC S147-V531
gC Y322-S523
gC Y419-S523
+ IFN-γ
E
Adhesion WT vs LFA KO
Cells/ROI
ns
ns
ns
***
WT
LFA-1 KO
unstimulated
gC S147-V531
no gC
gC S147-V531
+ IFN-γ

Figure 5

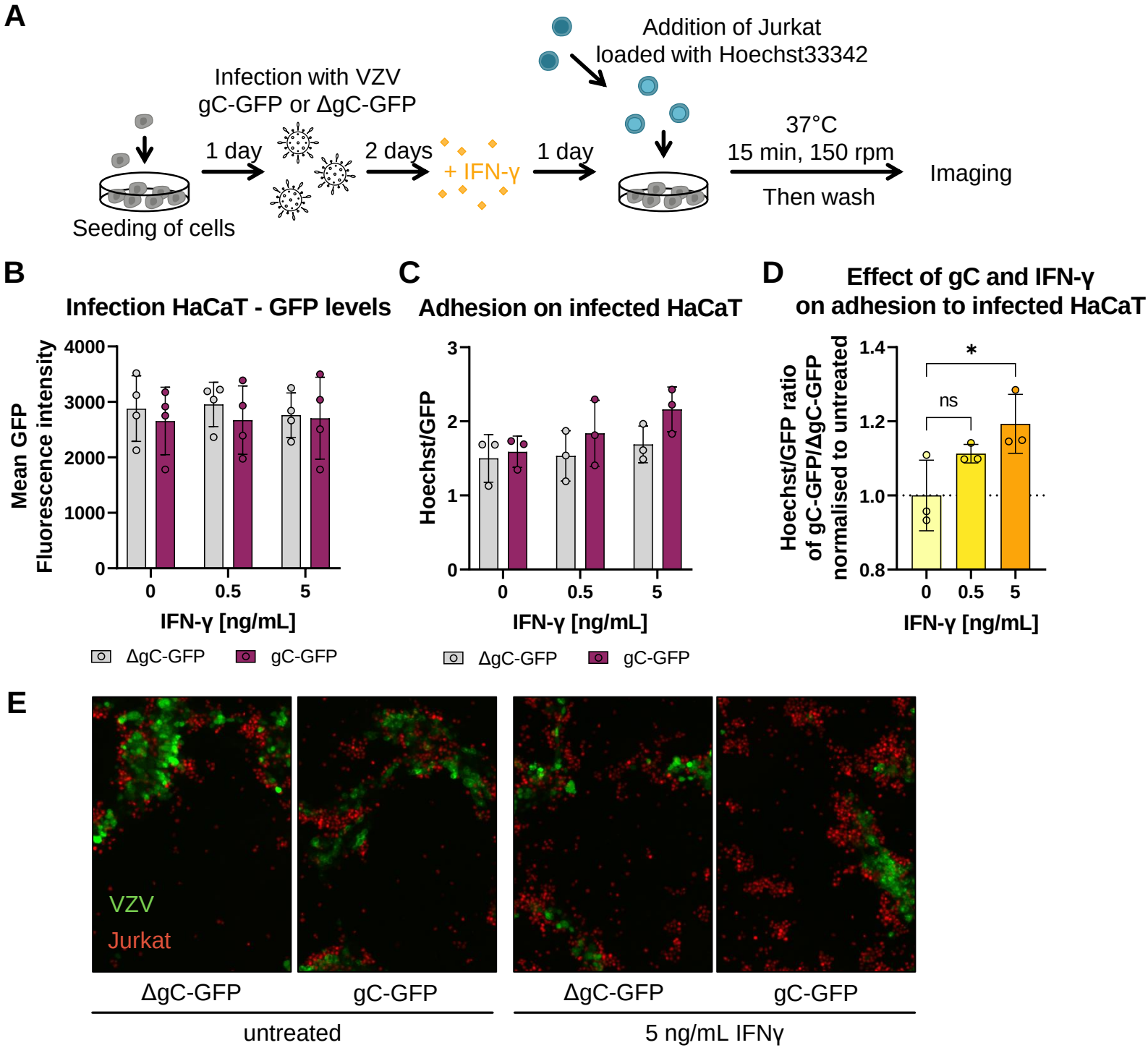
A
Addition of Jurkat
loaded with Hoechst33342
Infection with VZV
gC-GFP or ΔgC-GFP
1 day
2 days
+ IFN-γ
1 day
37°C
15 min, 150 rpm
Then wash
Imaging
Seeding of cells
B
Infection HaCaT - GFP levels
Mean GFP
Fluorescence intensity
4000
3000
2000
1000
0
0
0.5
5
IFN-γ [ng/mL]
ΔgC-GFP
gC-GFP
C
Adhesion on infected HaCaT
Hoechst/GFP
3
2
1
0
0
0.5
5
IFN-γ [ng/mL]
ΔgC-GFP
gC-GFP
D
Effect of gC and IFN-γ
on adhesion to infected HaCaT
Hoechst/GFP ratio
of gC-GFP/ΔgC-GFP
normalised to untreated
1.4
1.2
1.0
0.8
*
ns
0
0.5
5
IFN-γ [ng/mL]
E
VZV
Jurkat
ΔgC-GFP
gC-GFP
ΔgC-GFP
gC-GFP
untreated
5 ng/mL IFNγ

Figure 6

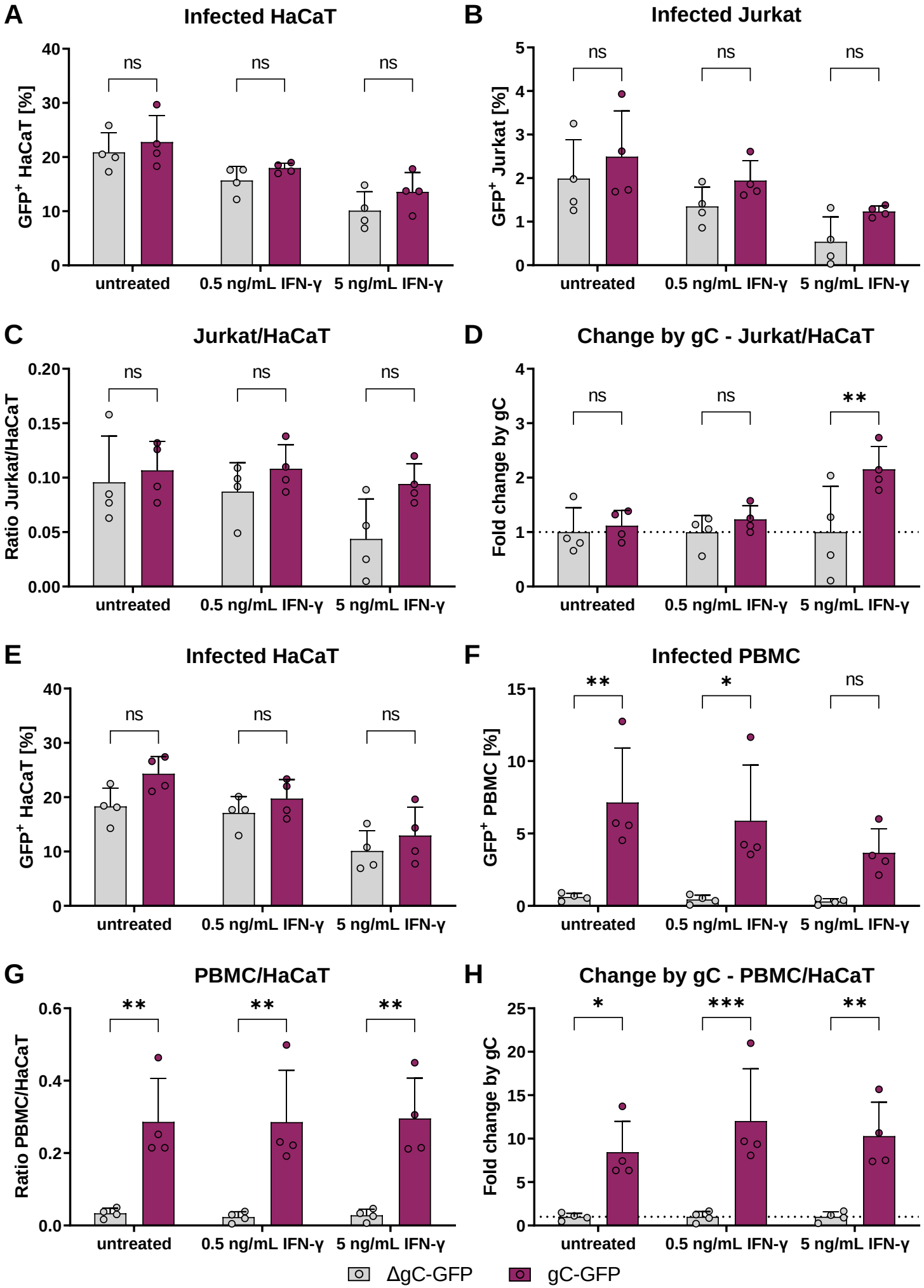
A
Infected HaCaT
GFP+ HaCaT [%]
ns
untreated
0.5 ng/mL IFN-γ
5 ng/mL IFN-γ
B
Infected Jurkat
GFP+ Jurkat [%]
C
Jurkat/HaCaT
Ratio Jurkat/HaCaT
D
Change by gC - Jurkat/HaCaT
Fold change by gC
**
E
Infected HaCaT
F
Infected PBMC
GFP+ PBMC [%]
*
G
PBMC/HaCaT
Ratio PBMC/HaCaT
H
Change by gC - PBMC/HaCaT
***
ΔgC-GFP
gC-GFP